



## Original Paper

# Construction of a foaming agent containing hydroxysulfobetaine and $\alpha$ -olefin sulfonate for clastic reservoirs with high temperature and high salinity



Long-Jie Li <sup>a, b</sup>, Ji-Jiang Ge <sup>a, b, \*</sup>, Peng-Fei Chen <sup>a</sup>, Peng-Ju Chu <sup>a</sup>

<sup>a</sup> School of Petroleum Engineering, China University of Petroleum (East China), Qingdao, 266580, Shandong, China

<sup>b</sup> Key Laboratory of Unconventional Oil and Gas Development, Ministry of Education, China University of Petroleum (East China), Qingdao, 266580, Shandong, China

## ARTICLE INFO

## Article history:

Received 6 December 2023

Received in revised form

13 November 2024

Accepted 13 November 2024

Available online 24 November 2024

Edited by Yan-Hua Sun

## Keywords:

Hydroxysulfobetaine

$\alpha$ -olefin sulfonate

Foaming agent

Solubility

Temperature and salinity resistance

Bulk foam test

Mobility control

## ABSTRACT

High-temperature and high-salt reservoirs are often accompanied by serious gas channeling in gas flooding, which will greatly affect the effect of gas injection development, so in-situ foaming of temperature-resistant and salt-resistant foaming agents is commonly used to control gas channeling. The feasibility of the compound system of dodecyl hydroxyl sulfobetaine (HSB12) and  $\alpha$ -olefin sulfonate (AOS) as foaming agent for sandstone reservoir was studied at 130 °C and  $22 \times 10^4$  mg/L. The results showed that the foaming agent (HSB12 and AOS were compounded in a 6:1 mass ratio, in this article, this foaming agent is simply referred to as SA61) had good solubility in  $22 \times 10^4$  mg/L simulated formation water. Besides, the foaming volume of SA61 and HSB12 was similar, but the foam decay half-life of SA61 was 10–25 times higher than that of HSB12. The foaming performance of SA61 on the surface of quartz sand remained above 90% of that before adsorption. The strong interaction between HSB12 and AOS in the compound system SA61 was demonstrated by surface rheological measurements and NMR studies of surfactants. The results of core flow test showed that SA61 had better mobility control ability than HSB12 under the same surfactant concentration. In addition, SA61 showed a selective mobility reduction in 2005.30 and 632.00 mD cores. The above research results can guide the selection and application of foaming agent in clastic reservoir.

© 2025 The Authors. Publishing services by Elsevier B.V. on behalf of KeAi Communications Co. Ltd. This is an open access article under the CC BY-NC-ND license (<http://creativecommons.org/licenses/by-nc-nd/4.0/>).

## 1. Introduction

In the Tarim Tanan and Hade areas of China, there exist numerous clastic oil reservoirs characterized by high temperatures, high salinity, and medium-low permeability. Following prolonged water injection and oil extraction processes, these reservoirs necessitate gas injection for enhanced oil recovery. However, challenges arise due to formation nonhomogeneity, variations in gas–liquid viscosity, and disparities in gas–liquid density which make the gas injection process susceptible to gas channeling, thereby reducing overall efficiency of gas utilization (Li et al., 2024a). Consequently, foam application becomes imperative for effective deep mobility control and prevention of gas channeling in

such reservoirs (Lu, 2024; Wang et al., 2021). The well area mentioned has a temperature exceeding 120 °C and the formation water has a salinity surpassing  $22 \times 10^4$  mg/L, thus requiring a foaming agent that remains stable under high-temperature and high-salinity conditions. Betaine surfactants and strongly hydrophilic anionic surfactants, such as alkyl diphenyl ether disulfonates and alkyl sulfonates with carbon chains containing less than 10 carbons, are typically characterized by their excellent solubilities in brine with a salt concentration of  $22 \times 10^4$  mg/L (Mannhardt and Novosad, 1991). However, due to the limited foaming capabilities of alkyl diphenyl ether disulfonates and alkyl sulfonates with carbon chains shorter than 10 carbons, betaine was employed in this study to formulate surfactants compatible with high-temperature and high-salinity reservoirs. In medium and low permeability clastic reservoirs, the gravity overcovering caused by formation heterogeneity and the viscous fingering of the foam system are the main reasons for the rapid gassing and gas channelling of the foam

\* Corresponding author.

E-mail address: [gejijiang@163.com](mailto:gejijiang@163.com) (J.-J. Ge).

## Nomenclature

CMC	Critical micelle concentration, wt%
$D$	Diffusion coefficient, $10^{-9} \text{ m}^2/\text{s}$
PV	Pore volume
$t$	Observation time, min or h
$t_1$	Liquid drainage half-life, min or h
$t_2$	Foam decay half-life, min or h
$V$	Foaming volume, mL
$V_f$	Foam volume, mL
$V_l$	Liquid drainage volume, mL
$\Delta P$	Pressure differential generated at both ends of the rock core during the gas–liquid co-injection stage, kPa
$\Delta P_{\max}$	Maximum pressure differential generated at both ends of the rock core during the gas–liquid co-injection stage, kPa
$\Delta P_{\min}$	Minimum pressure differential generated at both ends of the rock core during the gas–liquid co-injection stage, kPa
$\Delta P_{\text{av}}$	Average value of the pressure difference generated at both ends of the rock core during the gas–liquid co-injection stage, kPa
$\Delta P_{\text{eq}}$	Average value of the pressure differential generated at both ends of the rock core during gas–liquid co-injection that reaches a relatively stable or equilibrium stage, kPa
$\delta$	Chemical shift, ppm

system. The reservoir space of carbonate reservoirs mainly includes karst caves, cavities and fractures, which are not conducive to the in-situ foam formation of foaming agents in the formation and the subsequent regulation of gas channeling. The foam is mainly sealed by reducing the relative permeability of the gas phase, profile control, gas floating and flooding, selectivity of crude oil, fluidity control and emulsification. The foam system is of great significance in the field of deep reservoir sealing, especially in low permeability/tight reservoirs, and its performance evaluation index and plugging ability have been significantly improved (Xu et al., 2024). Therefore, it is recommended to use foaming agents to generate foam in medium and low permeability clastic rock reservoirs to control gas channelling and improve the effect of gas injection development. Due to salt tolerance and other problems, few scholars would be compound long-chain anionic surfactants (such as  $\alpha$ -olefin sulfonate ( $C_{14-16}$ AOS)) with short-carbon chains and other amphoteric surfactants to construct high-salt resistant foaming agents. In addition, it is rarely reported that the foam decay half-life of the foaming agent constructed by the simple surfactant compound exceeds 24 h under high temperature, high pressure and high salt (Affi et al., 2021; Hanamertani et al., 2023), and many foaming agents such as particles and polymers are added with good foam decay half-life (Zhou et al., 2020).

The combination of betaine and anionic surfactants has been extensively studied, revealing significant synergistic effects. Pan et al. (2018) used SFG-VS to investigate the effects of equimolar betaine–ionic surfactant mixtures on water structure at the gas–liquid interface and found that interfacial water molecules were more ordered due to strong electrostatic interactions between the head groups of betaine and anionic surfactants. Molecular simulations showed that betaine enhances the density of the adsorbed layer by interacting with hydrophilic groups of AEC through its positively charged centers, thereby increasing interfacial film strength (Gao et al., 2017). Complexation reactions between anionic and betaine-based surfactants typically exhibit positive synergistic effects based on stronger electrostatic effects resulting from anionic surfactants and positively charged centers of betaines (Milton et al., 2015). Hines et al. (1997) observed a significant synergistic effect in reduced surface tension and critical micelle formation when investigating SDS and C12-betaine in distilled water at different temperatures. Danov et al. (2004) also observed a remarkable decrease in CMC for mixed systems along

with increased surface dilatation modulus upon adding small amounts of betaine to SDS while investigating their adsorption behavior at the gas–liquid interface in a medium containing NaCl at pH 5.5.

When selecting foaming agents, the adsorption performance of the agent on the rock surface is a crucial factor to consider. The lower the adsorption of the agent on the rock surface, the easier its migration in reservoirs, which is advantageous for deep-reservoir mobility control. Clastic rock reservoirs typically exhibit a negative surface charge, resulting in betaine surfactant molecules being adsorbed on negatively charged sandstone surfaces in a "V" shape with closely positioned positive centers and distanced negative centers. Consequently, betaine foaming agents demonstrate higher adsorption capacity on sandstone surfaces compared to anionic foaming agents. Moreover, due to its relatively high cost, general betaine is not commonly selected as a foaming agent for sandstone reservoirs. Previous research suggests that combining anionic surfactants such as  $\alpha$ -olefin sulfonate (AOS), sodium dodecyl sulfate (SDS), internal olefin sulfonate (IOS), etc., with betaine surfactants like dodecyl betaine and lauramid betaine not only enhances foam stability but also facilitates utilizing betaine surfactants as co-solvents for anionic surfactants, thereby improving their tolerance to high salinity (Gao et al., 2017; Hadian Nasr et al., 2020; Mumtaz et al., 2015; Syed et al., 2019). Consequently, developing a foaming agent system comprising  $\alpha$ -olefin sulfonate ( $C_{14-16}$ AOS) and dodecyl hydroxysulfobetaine (HSB12) can significantly enhance solubility of anionic surfactants in high-salinity water while exhibiting excellent foaming performance and reducing the adsorption capacity of betaine molecules on rock surfaces. The ratios of the two components were determined in this study by investigating their solubilities. Subsequently, the foaming performance and mobility control of the composite system were discussed through bulk foam tests and core flow experiments. The results demonstrate that the addition of a small amount of AOS to HSB12 in high-salinity water can significantly enhance the foaming performance of HSB12. The evaluation data on bulk foam and flow foam presented herein are valuable for guiding the selection and application of foaming agents in high-temperature and high-salinity reservoirs.

In this paper, the properties of the foaming agent were comprehensively studied, firstly, the solubility in the formation water with high salt content was used as the evaluation index to

complete the construction of the compound system, and then the bulk foam performance of the compound foaming agent before and after adsorption under the conditions of high temperature, high pressure and high salt in the formation was fully evaluated by using the new high-temperature and high-pressure foam evaluation instrument developed by the research group, and then the interaction mechanism of the compound system was clarified by means of surface rheology and NMR research. Finally, the foaming performance and mobility control performance of the foaming agent in porous media were investigated through core flow experiments, which laid a foundation for the popularisation and use of the compound foaming agent in the oilfield field.

## 2. Experimental section

### 2.1. Instruments, chemicals, and materials

The chemicals used in the experiments included analytically pure NaCl, CaCl<sub>2</sub>, MgCl<sub>2</sub>·6H<sub>2</sub>O, NaHCO<sub>3</sub>, cetyltrimethylammonium bromide, trichloromethane, as well as  $\alpha$ -olefin sulfonate (AOS1416, with a lipophilic group containing 14–16 carbons, abbreviated AOS or C<sub>14–16</sub>AOS), 3-(*N*-dodecyl-*N,N*-dimethyl)-2-hydroxypropylsulfobetaine (carbon chains containing 12–14 carbons, abbreviated as dodecyl hydroxysulfobetaine or HSB12), 3-(*N*-octadecyl-*N,N*-dimethyl)-2-hydroxypropylsulfobetaine (carbon chains containing 16–18 carbons, abbreviated as octadecyl hydroxysulfobetaine or HSB18). The chemical structures of the surfactants are shown in Fig. 1.

The simulated oilfield water used for the experiments was prepared according to the ion compositions shown in Table 1. The basic parameters of the long Berea cores used for the physical simulation experiments are shown in Tables 2 and 3.

The instruments used in the experiments included an LC-10A high-pressure liquid chromatograph (Shimadzu, Japan), a K100C

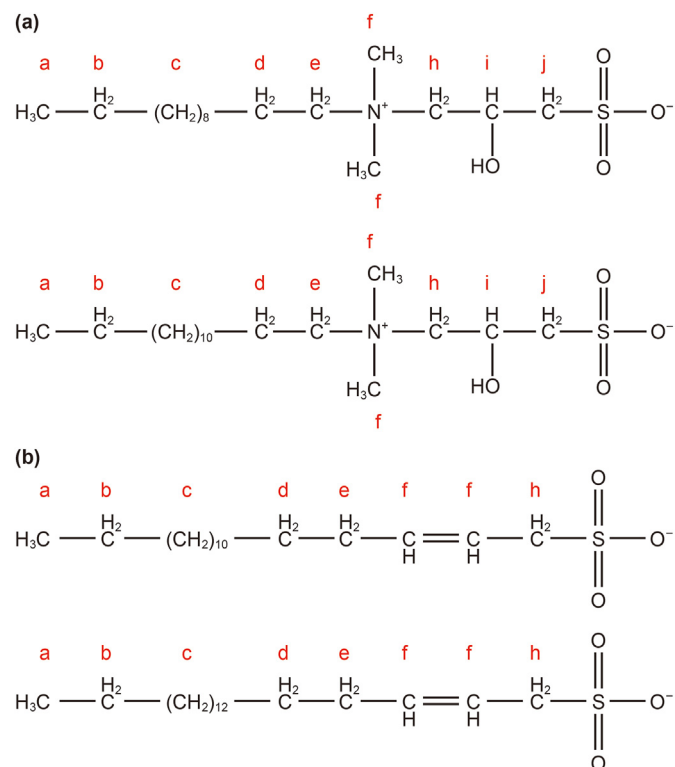


Fig. 1. Chemical structures of the surfactants used in these experiments: (a) HSB12; (b) C<sub>14–16</sub>AOS.

surface tension meter (KRÜSS, Germany), a DSA100 droplet shape analyzer (KRÜSS, Germany), an HCPM-III high-temperature and high-pressure foam evaluator (Nantong Xinhua Cheng Scientific Research Instrument Co., Ltd., China), a TY-4 core holder (Hai'an Yaxin Scientific Research Instrument Factory, China), an F-240MI gas mass flow controller (Beijing Hammer Technology Co., Ltd., China), a 100DX TELEDYNE ISCO high-precision piston pump (Wuhan Aolebo Science and Technology Co., Ltd., China), a DP1300-DPHFA3DPN1N1N Senex differential pressure gauge (Guangzhou Senex Instrument Co., Ltd., China), a model 26-1061-24-008 high-pressure reducing valve (Emerson Process Control Group of the U.S.A.), and a ZR-3A high-temperature and high-pressure intermediate vessel tank (Hai'an Yaxin Scientific Research Instrument Factory, China).

### 2.2. Experimental methods

#### 2.2.1. Evaluation of surfactant foaming performance

2.2.1.1. *Before adsorption.* The bulk foam test for different foaming agents was conducted at 130 °C and 30 MPa using the HCPM-III high-temperature and high-pressure foam evaluator (Li et al., 2024b, 2024c). The experimental procedure was as follows: Initially, the foam evaluator was filled with 100 mL of foaming agent solution prepared using simulated formation water. The sealing cover of the foam instrument was securely fastened, and temperature and pressure sensors were inserted into the cell. Gas was then introduced into the evaluator's cell up to 80% of the desired experimental pressure. Subsequently, the heating switch on the control system of the foam instrument was activated to uniformly heat both upper and lower regions of the instrument until reaching the target temperature using an electric heating jacket. Finally, by adjusting the safety valve, precise regulation of pressure inside the cell matching with desired value was achieved. Following this adjustment, a stirring rotor within the cell was set at a speed of 2500 r/min for 1 min using a speed-control knob. After cessation of stirring, prompt inversion of the foam evaluator allowed visual observation through glass windows while contemporaneously recording alterations in both foam volume and liquid drainage volume. The initial foaming volume, denoted as *V*, was determined immediately after stirring completion. The liquid drainage half-life, represented by *t*<sub>1</sub>, was defined as the time required for the liquid volume to decrease to half of its original value. Similarly, the foam decay half-life, represented by *t*<sub>2</sub>, was defined as the observation time required for the foam volume to decrease to half of its original value.

2.2.1.2. *After adsorption.* Initially, the quartz particles underwent acid-washing, followed by water rinsing and subsequent drying. A solution of foaming agent was prepared using simulated formation water with a specific concentration. The quartz sand and foaming agent solution were then combined at a solid–liquid mass ratio of 1:3, placed in an ampoule, and aged at 130 °C for 24 h. After completion of the aging process, the foaming agent solution was rapidly cooled to room temperature and filtered to separate it from the quartz sand. Subsequently, the high-temperature and high-pressure foam evaluator was utilized to assess the bulk foam performance of the adsorbed foaming agent using experimental methods outlined in Section 2.2.1.1.

#### 2.2.2. Interface properties of the surfactants

2.2.2.1. *Measurement of the critical micelle concentration.* The surface tensions of the surfactants were measured using a K100C surface tensiometer (Metin et al., 2012). Initially, a series of surfactant solutions with varying concentrations were prepared in simulated formation water. Subsequently, each sample was

**Table 1**  
Ionic compositions of the simulated oilfield water.

Ionic composition, mg/L					Total salinity, mg/L
Na <sup>+</sup>	Ca <sup>2+</sup>	Mg <sup>2+</sup>	HCO <sub>3</sub> <sup>-</sup>	Cl <sup>-</sup>	
73296.20	11272.50	1518.20	183.60	137529.50	223800.00

**Table 2**  
Mineral compositions of the Berea cores.

Core number	Mineral composition and content, %								
	Quartz	Potassium feldspar	Plagioclase	Calcite	Dolomite	Siderite	Chabazite	Coesite	Clay
50-1 <sup>#</sup>	92.92	2.41	–	–	–	0.25	–	0.10	4.32
180-2 <sup>#</sup>	86.18	5.51	2.80	0.30	1.61	0.20	–	0.59	2.81
500-3 <sup>#</sup>	87.74	5.26	2.30	–	0.30	0.20	0.15	0.20	3.85
2000-1 <sup>#</sup>	89.99	3.99	2.28	–	0.10	0.10	–	0.10	3.44

**Table 3**  
Basic parameters of the Berea cores.

Core number	Length, cm	Diameter, mm	Dry weight, g	Wet weight, g	Porosity, %	$k_g^a$ , mD	$k_b^b$ , mD
50-1 <sup>#</sup>	29.38	25.00	320.69	344.51	14.49	46.50	6.87
180-2 <sup>#</sup>	30.07	25.10	315.88	344.79	17.05	185.50	13.51
500-3 <sup>#</sup>	29.18	25.00	277.22	305.92	17.58	632.00	83.92
2000-1 <sup>#</sup>	30.00	25.00	259.33	295.12	21.33	2005.30	256.28

<sup>a</sup> Gas measurement of core permeability.

<sup>b</sup> Brine measurement of core permeability.

subjected to three measurements of surface tension to obtain an average value and minimize experimental uncertainties. The resulting data was used to plot the surface tensions of the surfactant solutions against the logarithm of their concentrations. The abscissa value at the inflection point on this curve corresponded to the critical micelle concentration (CMC) of the surfactant.

**2.2.2.2. Measurement of the surface rheology.** The surface dilational rheology was measured using the oscillating drop module of the KRÜSS's DSA100 drop shape analyzer. The surface dilational modulus  $E$  was obtained from Gibbs' formula as the change in surface tension divided by the strain per unit area (Koelsch and Motschmann, 2005).

$$E = \frac{d\gamma}{d\ln A} \quad (1)$$

where  $E$  is the surface dilational modulus, mN/m;  $\gamma$  is the surface tension, mN/m; and  $A$  is the droplet surface area, m<sup>2</sup>.

The gas–liquid interfacial membrane exhibited elasticity due to the interactions between adsorbed surfactant molecules, while the surfactant molecules at the interface displayed distinct dynamic microscopic relaxation processes. Additionally, the interface also possessed a certain level of viscosity. Therefore, the dilational behavior can be described as a composite form of the elastic modulus  $E'$  and the viscous modulus  $E''$ .

$$E = E' + iE'' \quad (2)$$

$$E' = |E|\cos\theta \quad (3)$$

$$E'' = |E|\sin\theta \quad (4)$$

where  $E'$  is the dilatational elastic modulus, mN/m;  $E''$  is the dilatational viscous modulus, mN/m; and  $\theta$  is the phase angle, °.

The surfactant was initially dissolved in the simulated formation

water to obtain various concentrations. Subsequently, a droplet of suitable size was formed using a 2.5 mL syringe with the needle positioned at the bottom of the apparatus. Once adsorption equilibrium of surfactant molecules at the gas–liquid interface was achieved (surface tension measurements were taken every 10 min, and the standard deviation of surface tension differences between five consecutive measurements was less than 0.005 mN/m), sinusoidal signals with constant frequency and volume changes were applied to the droplets using an oscillator, while their shapes were recorded by a video camera. Finally, based on variations in interfacial area and surface tension, calculations were performed to determine the surface dilational rheology of the system. In our experiments, we maintained a fixed frequency of 0.1 Hz for sinusoidal oscillation signals and controlled amplitude change rate of droplet interfacial area at 5%.

### 2.2.3. Evaluation of foaming performance in porous media with flow experiment

The foam resistance factor was determined by injecting a foaming agent solution (or simulated salt water) and gas into the Berea core at a specific velocity, with the stable equilibrium value of foam formation in the core obtained from small pressure fluctuations. The resistance factor ( $F_R$ ), apparent viscosity ( $\mu$ ), and relative mobility ( $\lambda_r$ ) of the foam were then calculated using Eqs. (5)–(7), respectively:

$$F_R = \frac{P_2}{P_1} \quad (5)$$

$$\mu = \frac{kA\Delta P}{QL} \quad (6)$$

$$\lambda_r = \frac{1}{\mu} = \frac{QL}{kA\Delta P} \quad (7)$$

where  $F_R$  is the foam resistance factor (dimensionless);  $P_1$  is the

equilibrium pressure difference formed by the foam at both ends of the core during gas–water co-injection, kPa;  $P_2$  is the equilibrium pressure difference formed by the foam at both ends of the core during gas–surfactant solution co-injection, kPa;  $k$  is the permeability of the core,  $10^{-3} \mu\text{m}^2$ ;  $\mu$  is the apparent viscosity of the foam, mPa·s;  $Q$  is the volumetric flow rate through the cross-section of the core,  $\text{cm}^3/\text{s}$ ;  $L$  is the length of the core, cm;  $A$  is the cross-section area of the core,  $\text{cm}^2$ ; and  $\Delta P$  is the pressure difference for the foams at both ends of the core,  $10^5 \text{ Pa}$ .

The thermostatted oven was set to a temperature of  $130^\circ\text{C}$  for the experiments, while the outlet back pressure of the core was adjusted to 10 MPa. The total gas and liquid injection had an apparent velocity of 6 m/day with a gas–liquid ratio of 4:1, as determined by the outlet back pressure measurement. The F-240MI gas mass flow controller regulated the gas injection rate, while an ISCO piston pump controlled the liquid injection rate. Additionally, a Senex differential pressure gauge measured the pressure difference between both ends of the core. After utilization, thorough rinsing with substantial quantities of simulated formation water was performed on the core before recycling it. Fig. 2 presents a flow chart illustrating the specific flow experiment conducted in this study (Li et al., 2024a). In Fig. 3(a), we observe the pressure difference at both ends of a Berea core after initial saturation with simulated formation water followed by co-injection of gas and simulated brine in a ratio of 4:1. Fig. 3(b) illustrates how co-injection of gas and a solution containing SA61 (HSB12 and AOS were compounded in a 6:1 mass ratio, in this article, this foaming agent is simply referred to as SA61) at a concentration of 0.2 wt% results in another pressure difference under similar conditions. When calculating foam resistance factor, apparent viscosity, and relative mobility formed by different foaming agent systems within cores, it is common practice to use only relative equilibrium or stable pressure differences ( $\Delta P_{\text{eq}}$ ) during stages involving co-injection of gas–surfactant solutions rather than averaging all observed pressures differences ( $\Delta P_{\text{av}}$ ) throughout this stage (as depicted by bidirectional arrows in Fig. 3). In Fig. 3, stage I

represents the rapid pressure increase phase of the system, while stage II corresponds to either the co-injection of gas and simulated formation water or the co-injection of gas and foaming agent solution. It can be observed from stage II that as gas and foaming agent solution are continuously injected into the core, the pressure difference between both ends generally exhibits an initial rise followed by a gradual decrease in magnitude. The increasing injection pressure difference indicates an augmented number of liquid films formed within the core, which aligns with a progressive enrichment of foam at the core outlet. Upon examining local pressure curves, it is evident that the pressure difference consistently demonstrates repeated fluctuations. Notably, a superior quality foaming agent results in larger amplitude fluctuations in pressure difference. This phenomenon may be attributed to liquid film stretching through pore throats and has been suggested to involve competition between foam generation and foam coalescence (Afifi et al., 2021; Hanamertani et al., 2023; Xiong et al., 2022). In this context,  $\Delta P_{\text{eq}}$  can be selected and substituted into Eqs. (5)–(7) for calculating parameters such as resistance factor, apparent viscosity, and relative mobility of foam.  $\Delta P_{\text{eq}}$  denotes a relatively stable pressure drop during gas–liquid co-injection stage—specifically referring to average pressures within the range indicated by black bidirectional arrows in Fig. 3 with corresponding pressure drop range expressed using black font.

The Berea core was reused in the experiment. A substantial quantity of simulated formation water should be employed to thoroughly rinse the utilized core for each gas–liquid injection, and appropriate heating should be applied to ensure complete removal of foaming agent from the core pores during flushing towards the outlet end. Following core rinsing, 20 PV of formation water should be reinjected to prevent foaming. The effluent from the core should be collected every 5 PV injection and quantified using a surface tensiometer. When the standard deviation of surface tension is less than 1 mN/m for three consecutive measurements, it indicates that thorough cleaning has been achieved and enables reuse of the core.

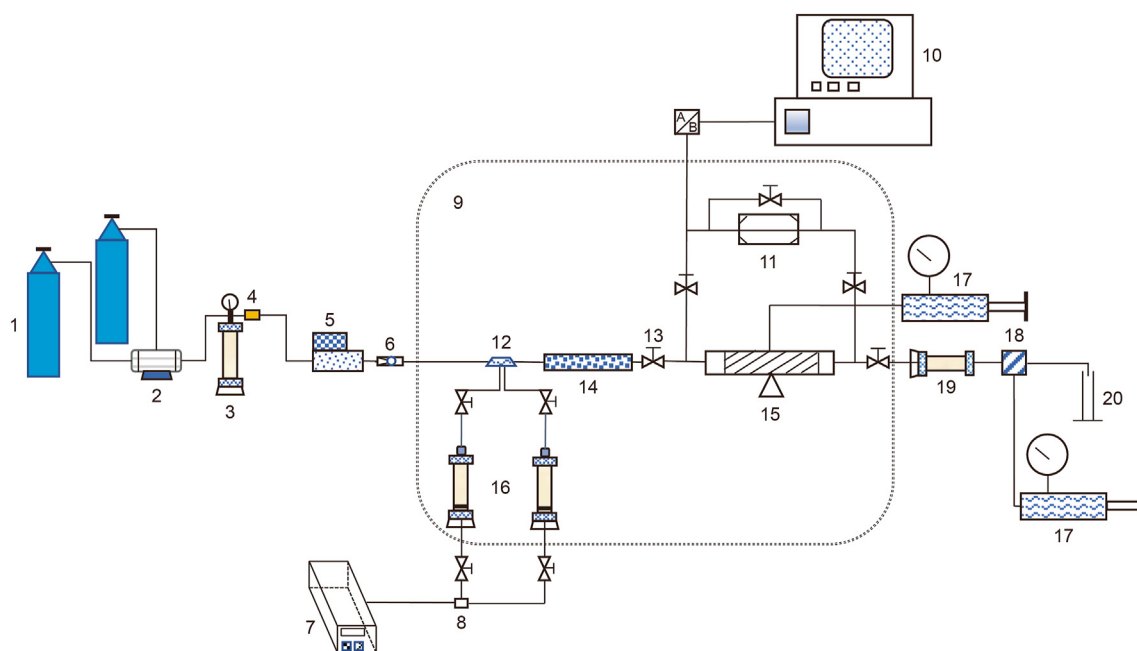


**Fig. 2.** Flow chart for the flow experiments. 1-gas source; 2-booster pump; 3-high-pressure storage tank; 4-pressure reducing valve; 5-gas mass flow controller; 6-check valve; 7-ISCO piston pump; 8-three-way valve; 9-constant temperature oven; 10-pressure acquisition system; 11-differential pressure gauge; 12-six-way valve; 13-valve; 14-foam generator (a sandpack filled with quartz sand to simulate the porous medium of the formation); 15-high-temperature and high-pressure core holder; 16-temperature and pressure-resistant intermediate vessel tank; 17-hand pump; 18-back-pressure valve; 19-buffer vessel tank; 20-volumetric cylinder.

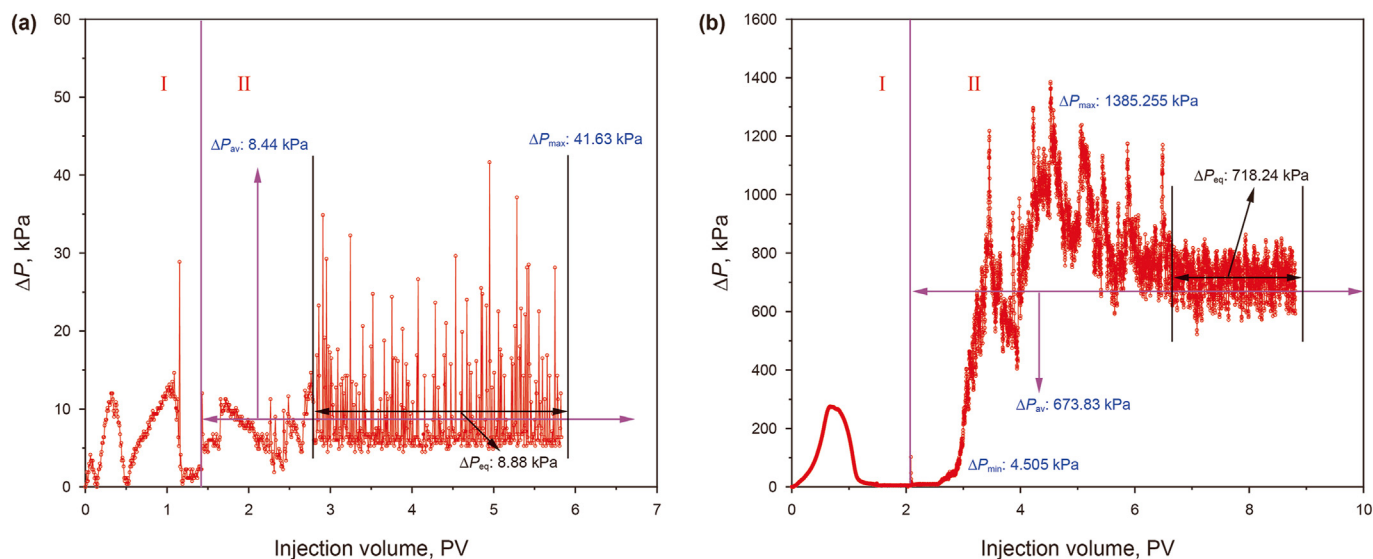


**Fig. 3.** Differential pressure change at both ends of the core after co-injection of saturated simulated formation water and gas–liquid with a gas–liquid ratio of 4:1: (a) simultaneous injection of  $22 \times 10^4$  mg/L simulated formation water and gas; (b) simultaneous injection of 0.2 wt% SA61 and gas. I: simulated formation water/surfactant solution injection and pressurization; II: gas–simulated formation water/surfactant solution co-injection.

### 3. Experimental results and discussion

The combination of betaine surfactants and anionic surfactants exhibits synergistic effects, thereby enhancing their performance. We selected dodecyl hydroxysulfobetaine (HSB12) and  $\alpha$ -olefin sulfonate ( $C_{14-16}$ AOS) as the components for formulating a foaming agent suitable for operation at a temperature of 130 °C with a salinity content of  $22 \times 10^4$  mg/L. The ratio between these two components was determined based on solubility analysis, followed by an investigation into the foaming performance and mobility control capability of the composite system through bulk foam tests and core flow experiments.

#### 3.1. Compound surfactant construction

Firstly, the solubility of the foaming agent in brine was evaluated. HSB12 demonstrated excellent solubility in water with a salinity of  $22 \times 10^4$  mg/L, as well as  $Ca^{2+}$  and  $Mg^{2+}$  concentrations of  $2 \times 10^4$  mg/L. In contrast, AOS encountered challenges when dissolving in water with a salinity of  $10 \times 10^4$  mg/L and  $Ca^{2+}$  and  $Mg^{2+}$  contents of  $1 \times 10^4$  mg/L. However, the addition of HSB12 significantly enhanced the solubilities of AOS in high-salinity water. Even at a temperature of 90 °C, when the compound ratio for HSB12 and AOS was set at 3:1, solubility remained low. At a ratio of 5:1, only a small amount of insoluble matter persisted after an extended period (15 days) at room temperature. Nevertheless, upon heating to 90 °C followed by cooling back down to room temperature, no precipitation occurred and a clarified solution formed. With a ratio of 6:1, the resulting system exhibited good solubility within the concentration range from 0.01 to 1 wt% in water with salinity levels reaching up to  $22 \times 10^4$  mg/L. Therefore, it was concluded that constructing a foaming agent resistant to both temperature and salinity would necessitate using HSB12 and AOS in a ratio of 6:1. In this article, this foaming agent is simply referred to as SA61. Fig. 4 shows the dissolution of HSB12 and AOS in simulated formation water at  $22 \times 10^4$  mg/L at different proportions and concentrations.

Additionally, the solubilization effect of long carbon chain hydroxysulfobetaine HSB18 on AOS was also investigated in this study. However, it was observed that HSB18, which shares a similar structure with HSB12, did not exhibit any solubilization effect on

AOS at both low and high temperatures, as depicted in Fig. 5.

The solubilization effects of HSB18 and HSB12 on AOS are influenced by the presence state of hydroxy sulfobetaine surfactant in brine, as well as the interaction between hydroxy sulfobetaine surfactant and AOS. The hydrophilic groups of hydroxy sulfobetaine surfactants can undergo self-folding, forming a thermodynamically favorable six-membered ring containing an intramolecular ion pair (Fig. 6(a)). However, under saline conditions, this ring may open up (Fig. 6(b)), resulting in two intermolecular ions instead of one intramolecular ion (Stournas, 1984; Ji et al., 2018). This situation creates conditions for the pairing between anionic surfactants and hydroxyl sulfobetaine (Jian et al., 2018). The matching carbon chains between HSB18 and AOS facilitate their pairing through van der Waals attraction between lipophilic groups and electrostatic attraction between hydrophilic groups. As a result, a complex is formed that exhibits low solubility in high-salinity water (Fig. 6(c)). On the other hand, due to the mismatching carbon chain with AOS's carbon chain, HSB12 shows weak pairing effect which does not readily precipitate from brine but can be solubilized in micelles formed by HSB12 (Fig. 6(d)). The formation of intermolecular compounds between anionic and zwitterionic surfactants in solid phases was also observed by Tsujii et al. (1982) during the measurement of Krafft points for binary mixtures.

#### 3.2. Evaluation of the foaming performance

##### 3.2.1. Measurement of foaming performance before adsorption

The foaming volume ( $V$ ), foam decay half-lives ( $t_2$ ), and liquid drainage half-lives ( $t_1$ ) of the foaming agents were determined using a high-temperature and high-pressure foam evaluator under simulated reservoir conditions to facilitate the selection of suitable foaming agents. Under high-temperature and high-salinity conditions, an effective foaming agent stabilizes the foam efficiently, resulting in an extended foam decay half-life. In 2020, Zhou et al. (2020) from Chevron reported that the half-life of foam decay for cocoamidopropyl betaine was approximately 12.5 h at a temperature of 85 °C, pressure of 34.5 MPa, and with a simulated brine containing  $Ca^{2+}$  and  $Mg^{2+}$  at a concentration of 5 wt%. Furthermore, the foam stability could be extended up to 24 h by incorporating a complex system consisting of cocoamidopropyl betaine,

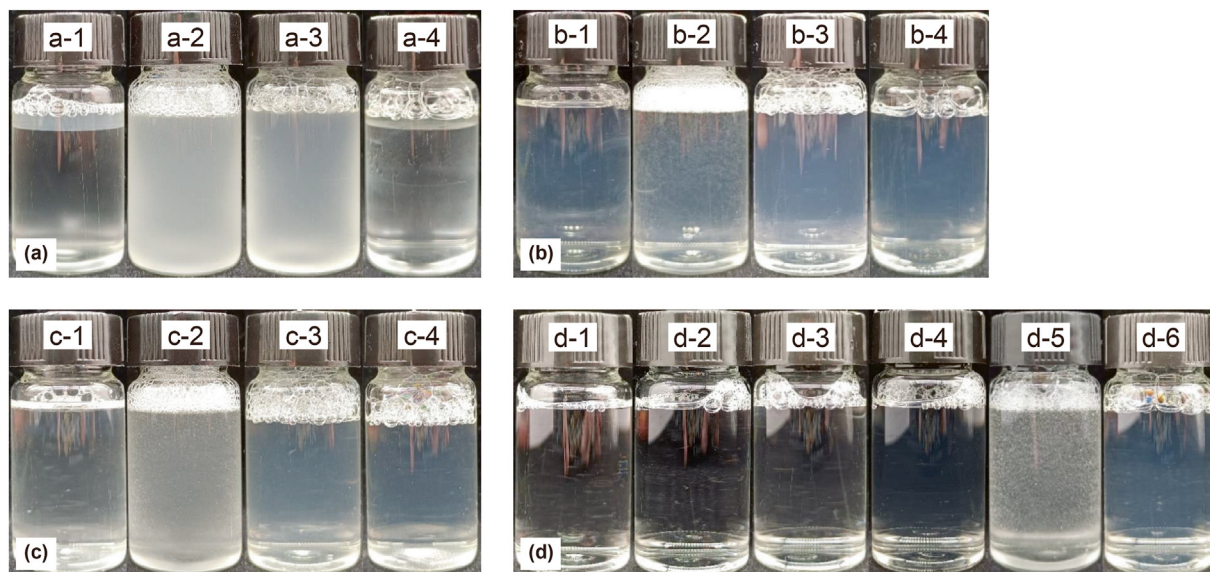


**Fig. 4.** Dissolution of HSB12 and AOS in simulated formation water at  $22 \times 10^4$  mg/L at different proportions and concentrations: (a) 1 wt% (HSB12:AOS = 3:1); (b) 1 wt% (HSB12:AOS = 5:1); (c) 1 wt% (HSB12:AOS = 6:1); (d) different concentrations of HSB12 and AOS were mixed in a 6:1 system. (a-1), (b-1), (c-1): the sample was left at room temperature for 15 days; (a-2), (b-2), (c-2): the sample was left at room temperature for 15 days and then gently agitated; (a-3), (b-3), (c-3): after being kept at room temperature for 15 days, it was then heated at 90 °C for 4 h; (a-4), (b-4), (c-4): after being kept at room temperature for 15 days, heated it at 90 °C for 2 h and then let it stand at room temperature for 12 h; (d-1) 0.01 wt% at ambient temperature; (d-2) 0.05 wt% at ambient temperature; (d-3) 0.1 wt% at room temperature; (d-4) 0.5 wt% at room temperature; (d-5) 1 wt% at ambient temperature; (d-6) 1 wt% at 90 °C for 1 h and then standing at room temperature.

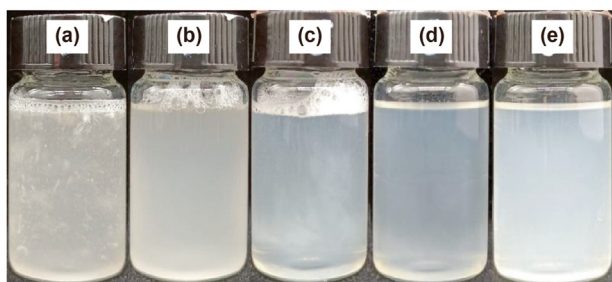


**Fig. 5.** Dissolution of HSB18 and AOS in a system with a mass ratio of 6:1 at different conditions: (a) 1 wt% at ambient temperature; (b) 1 wt% at 90 °C for 1 h; (c) 1 wt% at 90 °C for 12 h; (d) 1 wt% at 90 °C for 64 h; (e) 1 wt% at 90 °C for 5 d.

AOS, and a nonionic surfactant (Zhou et al., 2020). The foaming capabilities of surfactant solutions with a concentration of  $5 \times 10^3$  mg/L were assessed in brine with a concentration of  $2 \times 10^5$  mg/L at a temperature of 90 °C and pressure of 13.8 MPa. The foam decay half-life for the foam generated using cocamidopropyl hydroxysulfobetaine and lauryl/myristyl amidopropylamine oxide was determined to be 1000 min (Afifi et al., 2021; Hanamertani et al., 2023). A comparison revealed that there have been limited reports on foam decay half-lives exceeding 48 h under simulated reservoir conditions with high salinity. The foaming capabilities of SA61 and HSB12 were evaluated and compared at 130 °C and 30 MPa. Figs. 7 and 8 illustrate the changes in foam volume ( $V_f$ ) and liquid drainage volume ( $V_l$ ) over observation time ( $t$ ) for different concentrations of SA61 and HSB12.

The foam volume underwent three distinct stages: rapid decay, steady decay, and slow decay, as observed in this study. The initial stage was characterized by a short duration with a nearly 25% decrease in foam volume and over 95% liquid drainage, indicating the dominance of gravity drainage as the primary mechanism for initial foam deterioration (Weaire et al., 1997). Subsequently, the dry foam entered a phase known as pseudo-plateau foam volume

(Simjoo et al., 2013), where no significant changes in foam volume occurred over time. Following this phase, the dry foam transitioned into a second period of gradual decay during which the foam volume slowly decreased. Fig. 9 presents an image captured from the window during SA61 evaluation to illustrate the appearance of the foam at that particular moment. It was widely accepted that changes in dry foam volume were associated with bubble coalescence and Ostwald ripening. On one hand, the surface tension of the foaming solution was low under high pressure. On the other hand, captured images revealed that dry foam exhibited a densely packed multilateral structure, and its volume was not directly correlated with liquid film curvature. Therefore, it could be inferred that the stability of hydroxy sulfobetaine-formed dry foam under elevated temperature and pressure primarily relied on foam coalescence. When the strength of the liquid film increased, its resistance to disturbances strengthens as well, resulting in a slower rate of foam coalescence and an extended half-life for foam decay.

The results depicted in Figs. 7 and 8 demonstrate that the foaming rate of SA61 was comparable to that of HSB12; however, SA61 exhibited exceptional foaming stability with a foam decay half-life that was 10–25 times longer than that of HSB12. Notably, the foam decay half-life for 0.1 wt% SA61 exceeded 3 days, which was rarely observed in existing literature on high-temperature and high-salinity conditions utilizing pure foaming agents. These findings suggested a significant synergistic effect resulting from the combination of dodecyl hydroxysulfobetaine and  $\alpha$ -olefin sulfonate.

### 3.2.2. Measurement of the foaming performance after adsorption

The adsorption of surfactants on the rock surface governs their propagation ability. Surfactants with high rates of adsorption exhibit limited penetration into the formation. Given that foaming agent is typically injected at a specific gas–liquid ratio, its dosage is significantly lower than that of compound flooding solutions, making the foaming agent's adsorption capacity crucial in regulating mobility. For surfactants used in alkali-surfactant-polymer

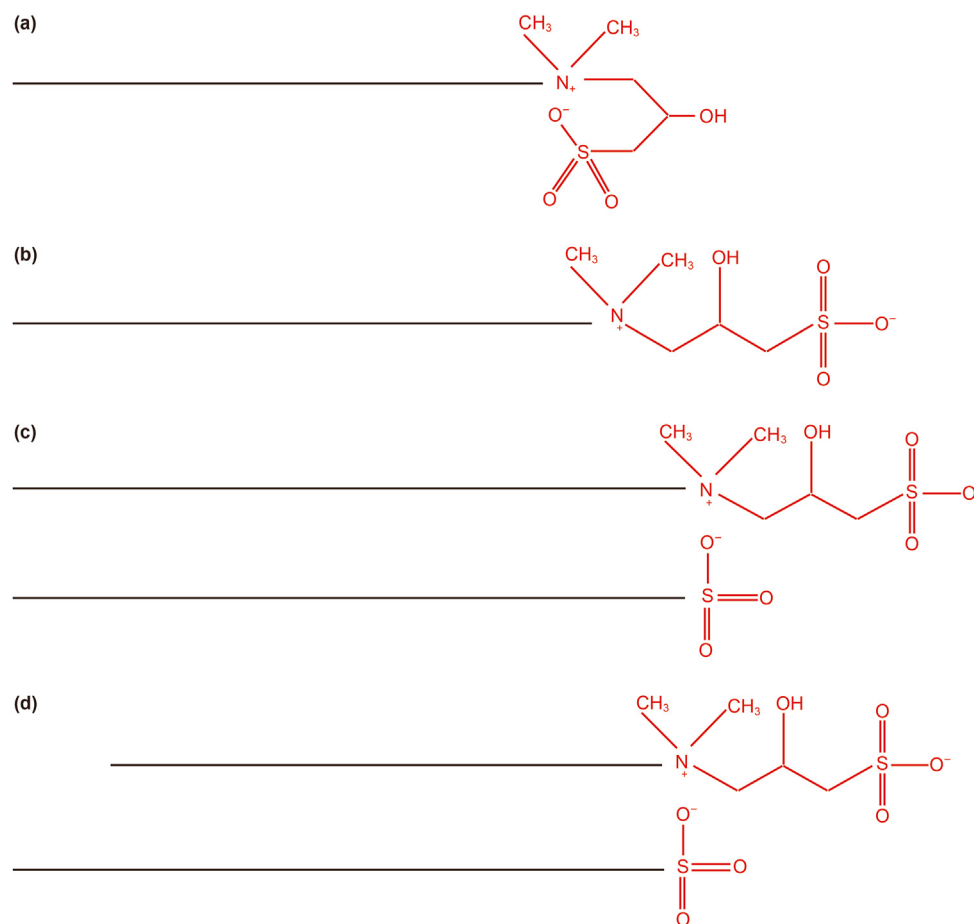


**Fig. 6.** The presence statuses of HSB12 and HSB18 in brine and their pairing with AOS. (a) The hydrophilic group of hydroxysulfobetaine folds into an intramolecular ion pair to form a thermodynamically stable six-membered ring. (b) The presence of ions in brine weakens the electrostatic attraction between ammonium and sulfonic acid groups, and the six-membered ring is destroyed. (c) HSB18 and AOS carbon chain length match, showing strong pairing effect, forming a complex that is insoluble in high-salinity water. (d) The lengths of the carbon chains of HSB12 and AOS do not match, the pairing effect is weak, and the mixed micelles are easy to form and will not precipitate immediately from the brine. The black line in the figure indicates that the saturated alkane chains with different carbon chain lengths, the longer the black line indicates that the carbon chain is also longer, and the molecular formula of the alkane chain can be uniformly expressed as  $C_nH_{2n+1}$ ; the red line in the figure indicates that it is a single bond of C–N, C–O, S–O and C–S.

ternary compound flooding in China, it is generally required that their static adsorption rate be below 1 mg/g (Q/SH1020 2191–2013, 2013). Similarly, for surfactants used in surfactant–polymer binary composite flooding (often referred to as alkali-free composite flooding), the static adsorption capacity must not exceed 2 mg/g (Zhu and Yang, 1994). Regarding foam flooding surfactants, Petro-China standards mandate that after being absorbed onto quartz sand surfaces, their foaming performance should remain above 85%.

The concentration of hydroxysulfobetaine surfactants can be determined by liquid chromatography, enabling the calculation of adsorption capacity. However, in the case of SA61, the strong interaction between HSB12 and AOS presents a challenge in their separation using a C18 silica gel column, thus impeding accurate determination of their concentrations. Consequently, this study focused on investigating the foaming properties of SA6 after its adsorption onto quartz sand surfaces. Fig. 10 illustrates the changes in foam volume and liquid drainage volume over time during the bulk foam test for SA61 following its adsorption on the surface of quartz sand. Fig. 11 compares the foaming volume, liquid drainage half-life, and foam decay half-life of the SA61 solution before and after adsorption on the quartz sand surface.

The foaming volume remained above 90% after adsorption, indicating that the compound surfactants had a low adsorption

capacity on sandstone surfaces. When the concentration of SA61 exceeded 0.1 wt%, the half-life for foam decay increased to over 4 days, representing a more than 25% enhancement compared to pre-adsorption conditions. This improvement could be attributed to the preferential adsorption of unreacted tertiary amines in SA61. These results demonstrated that SA61 exhibited exceptional foaming performance following static adsorption.

### 3.3. Determination of the surface tension and critical micelle concentration

The surface tensions of HSB12 and SA61 were determined at 30 °C with different concentrations, and the results are shown in Fig. 12. The critical micelle concentrations were  $1.42 \times 10^{-3}$  wt% and  $9.38 \times 10^{-4}$  wt%, respectively.

The combination of HSB12 with AOS resulted in a significant reduction in the critical micelle concentration (CMC), indicating an enhanced propensity for surfactant micelle formation. It is widely accepted that when the concentration of a surfactant solution surpasses a certain threshold, colloidal aggregates known as micelles are formed (Yin et al., 2007). This threshold concentration, at which the properties of the solution undergo a transition, is referred to as the critical micelle concentration (Zhao and Wang, 2010). Beyond CMC, excess surfactant monomers in the bulk

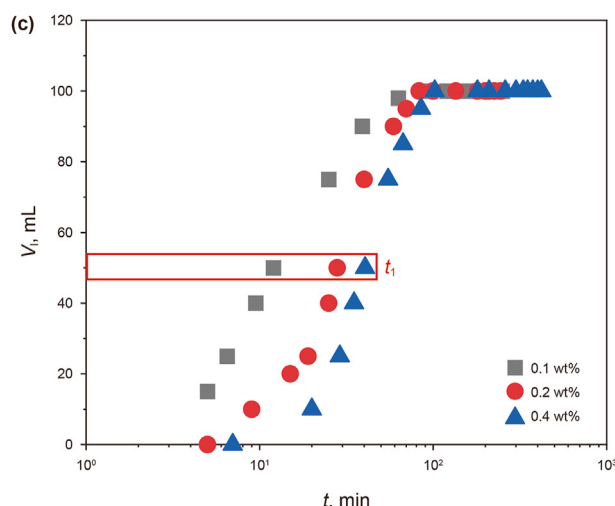
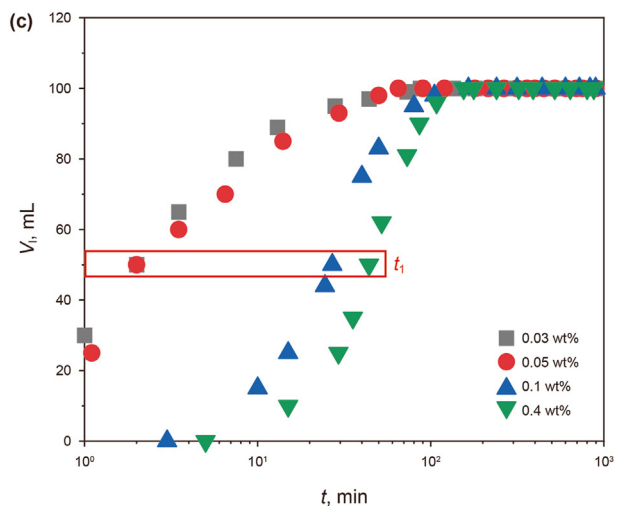
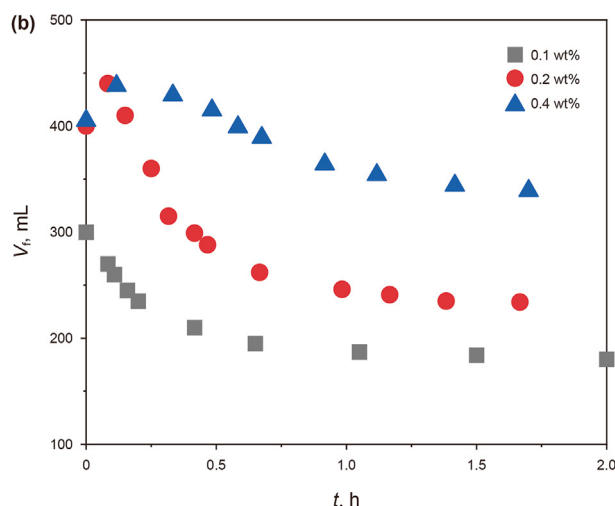
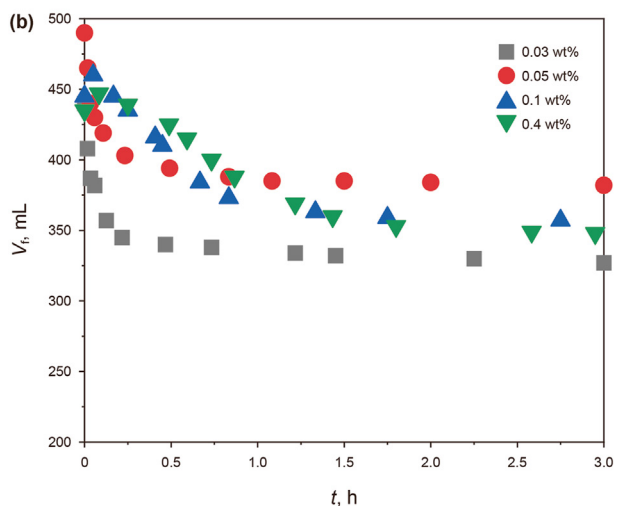
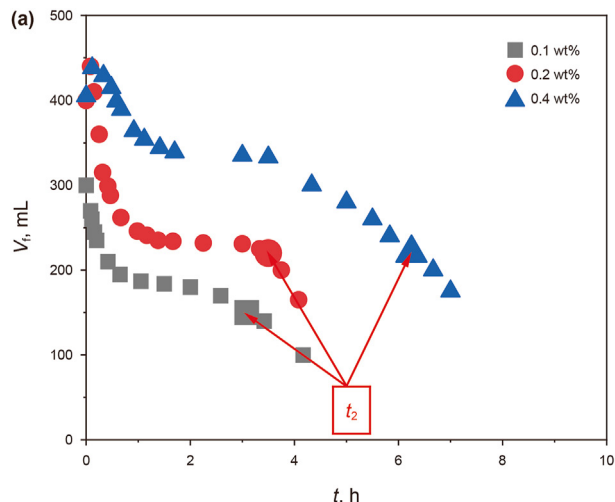
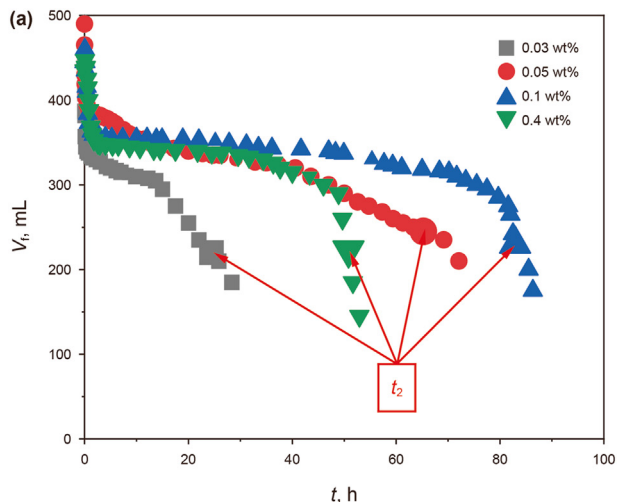


**Fig. 7.** Evaluation results of bulk foam properties for SA61 solution with different concentrations: (a) foam volume ( $V_f$ ) vs. observation time ( $t$ ); (b) foam volume vs. observation time (enlarge the horizontal coordinate); (c) liquid drainage volume ( $V_l$ ) vs. observation time.

**Fig. 8.** Evaluation results of bulk foam properties for HSB12 solution with different concentrations: (a) foam volume ( $V_f$ ) vs. observation time ( $t$ ); (b) foam volume vs. observation time (enlarge the horizontal coordinate); (c) liquid drainage volume ( $V_l$ ) vs. observation time.

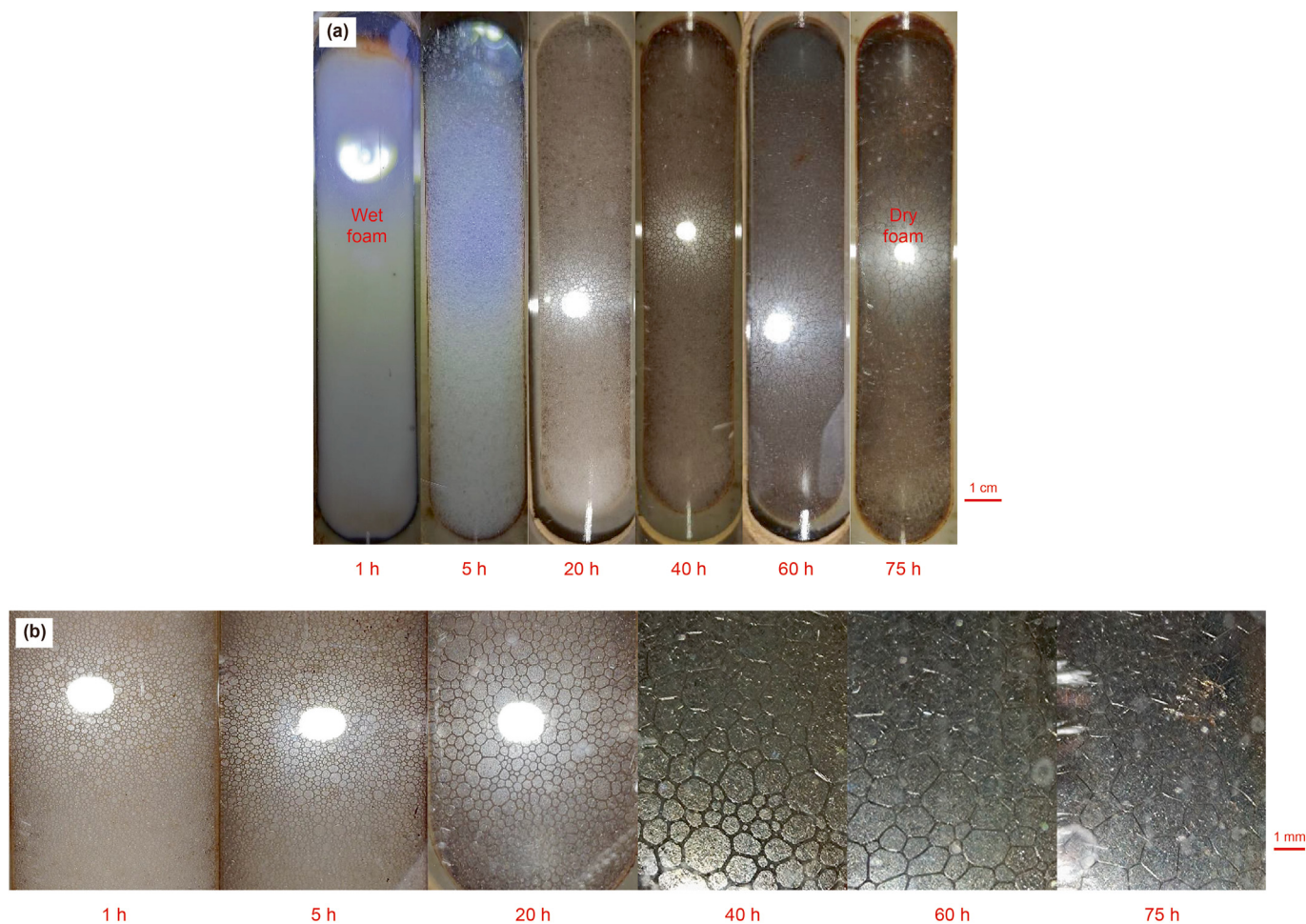


Fig. 9. Photos taken during the testing of 0.4 wt% SA61 bulk foam.

phase (liquid film) are more likely to aggregate into micelles after reaching adsorption equilibrium on gas–liquid interfaces during foam formation. This phenomenon not only contributes to improved stability of foam liquid films but also prolongs foam stability.

### 3.4. Surface rheology measurements

The main causes of foam destruction include liquid film drainage, Ostwald ripening, and coalescence of the liquid film. Previous evaluations of foam decay under high-temperature and pressure had shown that approximately 90% of the liquid drained within 40 min, resulting in the formation of dry foam. The polyhedral shape of these dry foams weakens Ostwald ripening caused by surface pressure differences. Therefore, the foam stability under high pressure is likely related to the ability of the liquid film to delay coalescence. Hence, it is necessary to investigate the strength of surfactant-formed liquid films. The surface dilational modulus can serve as an indicator for assessing how effectively a surfactant forms a surface film at gas–liquid interfaces. Physically speaking, the surface dilational modulus describes how much a surface tension increases when its area expands. A higher dilational modulus indicates greater resistance against perturbations and thus reflects better stability for a monolayer (Georgieva et al., 2009; Wang et al., 2017). Numerous experiments have demonstrated that the surface dilational modulus plays a crucial role in foam stability (Fruhner et al., 2000; Parra et al., 2019; Yu et al., 2019). Surface rheological

parameters resulting from different concentrations of HSB12 and SA61 in simulated brine were determined at 30 °C, and these results are illustrated in Fig. 13.

As illustrated in Fig. 13, when the surfactant concentration was significantly below the critical micelle concentration (CMC), the surface dilational viscosity modulus was considerably low, while the surface dilational elastic modulus exhibited a substantially higher value than the surface dilational viscosity modulus, indicating predominant elasticity during this stage. With an increase in surfactant concentration, viscoelastic behavior became evident in the surface film and reached its maximum near CMC. Generally, increasing concentration has dual effects on the dilational modulus. On one hand, a higher surfactant concentration results in more molecules adsorbed at the air/water interface, leading to stronger intermolecular interactions and consequently a greater surface dilational modulus. On the other hand, increased concentration enhances molecular diffusion exchange between bulk and surface film, resulting in reduced gradients of surface tension and a decrease in the surface dilational modulus (Yan et al., 2012; Lei et al., 2019; Shu et al., 2021). Additionally, when surpassing a surfactant concentration of 0.01 wt%, SA61 demonstrated a higher surface dilational modulus compared to HSB12, indicating enhanced film strength resulting from interactions between compound surfactants. This factor significantly contributed to superior foam stability achieved by SA61 as opposed to HSB12.

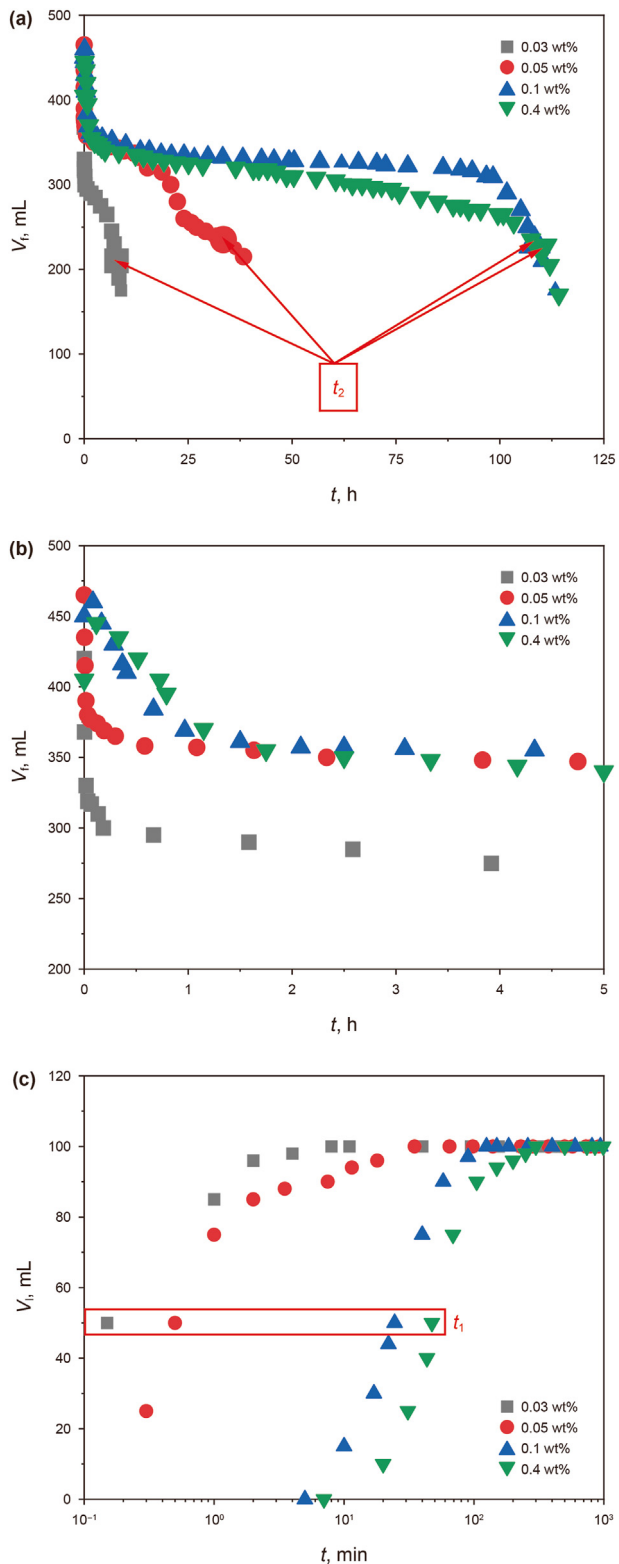


**Fig. 10.** Bulk foam test of SA61 solution after adsorption on quartz sand surface: (a) foam volume ( $V_f$ ) vs. observation time ( $t$ ); (b) foam volume vs. observation time (enlarge the horizontal coordinate); (c) liquid drainage volume ( $V_l$ ) vs. observation time.

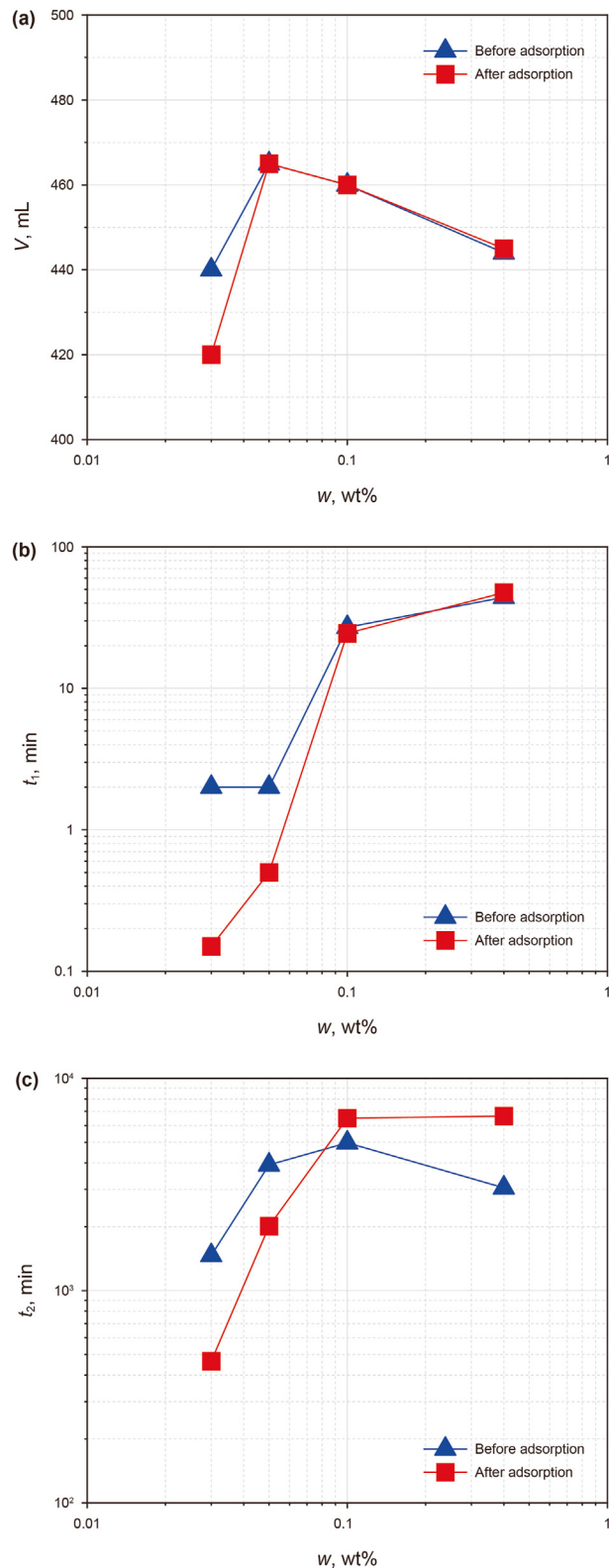


**Fig. 11.** Comparison of foaming properties of different concentrations ( $w$ ) of SA61 before and after their adsorption on the surface of quartz sand: (a) foaming volume ( $V_f$ ); (b) liquid drainage half-life ( $t_1$ ); (c) foam decay half-life ( $t_2$ ).

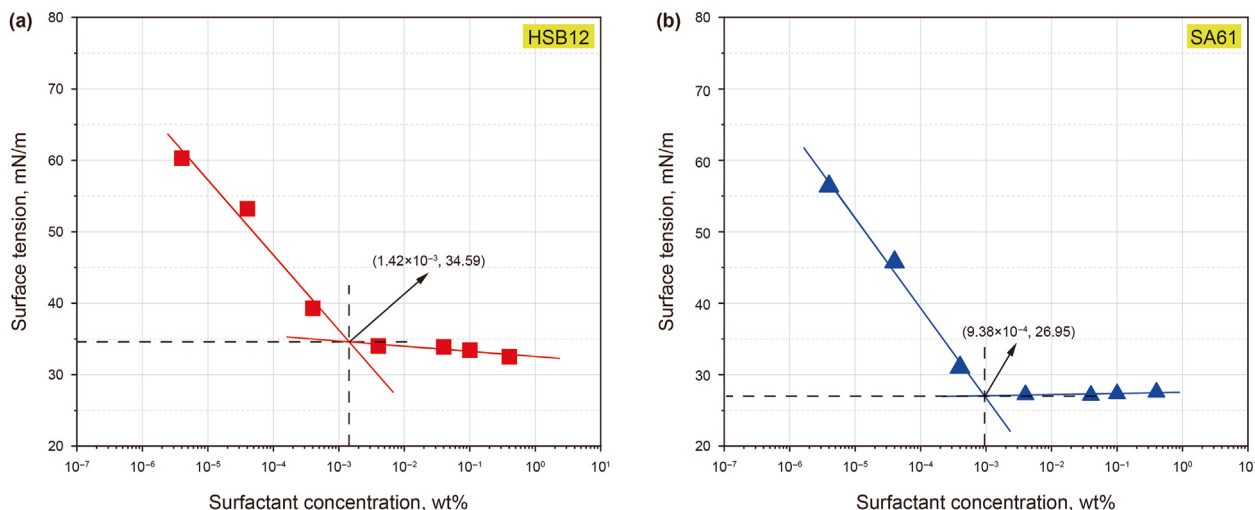


Fig. 12. Surface tension curves for different concentrations of HSB12 (a) and SA61 (b) in simulated formation water at 30 °C.

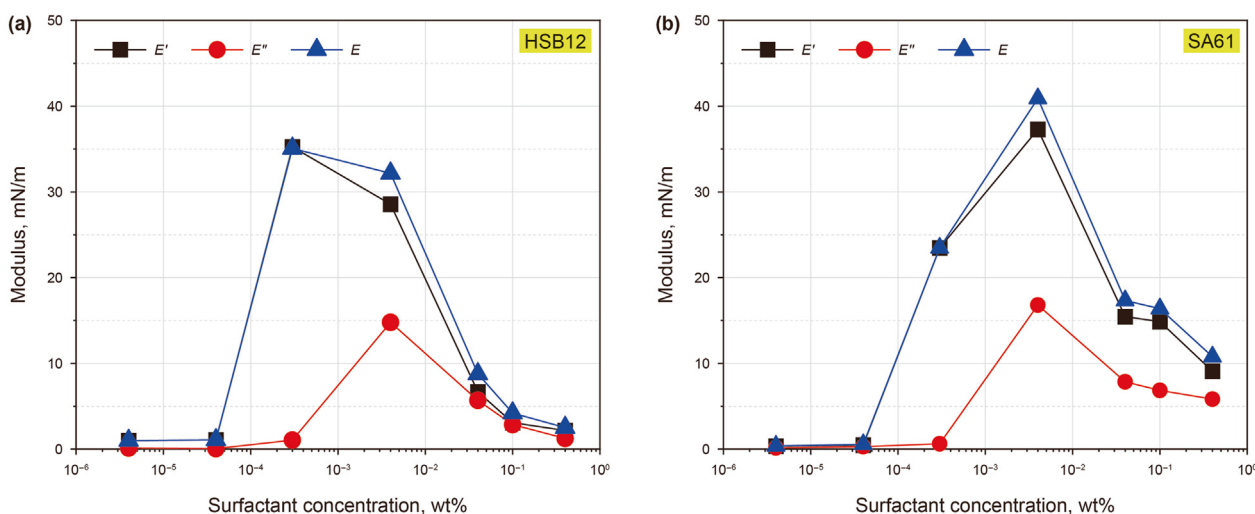


Fig. 13. Modulus of different concentrations of HSB12 (a) and SA61 (b) in simulated formation water.

### 3.5. NMR studies of the surfactant interactions

#### 3.5.1. DOSY measurements of different surfactants

To investigate the potential interaction between HSB12 and AOS, we conducted a one-dimensional diffusion ordered spectroscopy (DOSY) analysis of the compound system containing both surfactants. The  $^1\text{H}$  NMR spectra of different surfactants in Fig. 14 revealed distinct differences: the peak at  $\delta = 3.25$  ppm in Fig. 14(a) corresponding to HSB12 was absent in Fig. 14(a) for AOS, while conversely, the peak at  $\delta = 5.40$  ppm in Fig. 14(a) for AOS was not observed in Fig. 14(a) for HSB12. These characteristic peaks could be utilized to differentiate the diffusion coefficients ( $D$ ) of these two surfactants within the compound surfactant system. From Fig. 14(b), it is evident that the diffusion coefficient associated with  $\delta = 3.25$  ppm was determined as being approximately equal to  $1.22 \times 10^{-9} \text{ m}^2/\text{s}$ , whereas that corresponding to  $\delta = 5.40$  ppm was found to be around  $1.18 \times 10^{-9} \text{ m}^2/\text{s}$ ; remarkably close values were obtained for both cases. Furthermore, when examining the longitudinal coordinates (diffusion coefficients), it becomes apparent that they were centrally distributed along a straight line on this plot, indicating a strong interaction between these two surfactant molecules within this compound system.

#### 3.5.2. 2D $^1\text{H}$ – $^1\text{H}$ NOESY spectra demonstrating mixed surfactant interactions

To confirm the electrostatic attraction between HSB12 and AOS, we conducted 2D  $^1\text{H}$ – $^1\text{H}$  nuclear Overhauser effect spectroscopy (NOESY) of HSB12, AOS, and their composite systems. The NOESY spectra provided clear information about the proximity of intramolecular and intermolecular protons (Qi et al., 2016; McLachlan and Marangoni, 2010). Based on the  $^1\text{H}$  NMR comparisons shown in Fig. 14(a) for different surfactants at 25 °C, peaks for HSB12 and AOS appeared at  $\delta = 3.25$  ppm and  $\delta = 5.40$  ppm, respectively. The compound surfactant system's NOESY spectrum (Fig. 15(f)) contained cross-peaks that were not present in those of HSB12 or AOS (in red box), indicating an interaction between them. The new cross-peak in the compound system appeared at  $\delta = 3.25$  ppm corresponding to H proton in HSB12 (quaternary ammonium nitrogen-linked methylene). Therefore, there was indeed a gravitational interaction resulting from electrostatic attraction between positively charged quaternary ammonium nitrogen of HSB12 and negatively charged hydrophilic head group of AOS (Zhang et al., 2023).

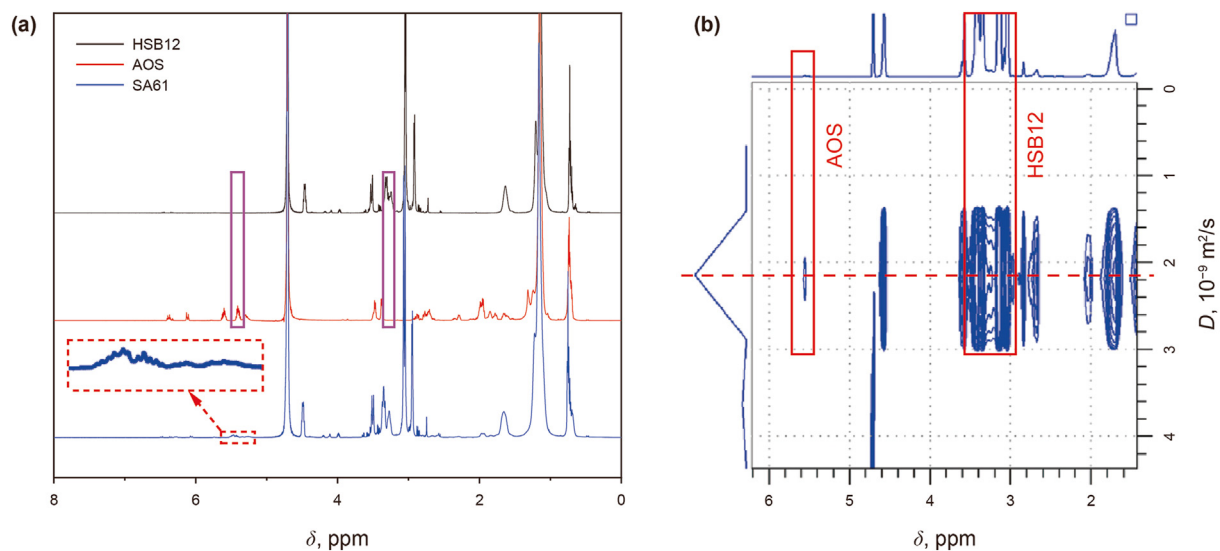


**Fig. 14.** Determination of the diffusion coefficients ( $D$ ): (a)  $^1\text{H}$  NMR comparison for different surfactants at 25 °C; (b) diffusion ordered NMR spectroscopy (DOSY) of the SA61 compound system.

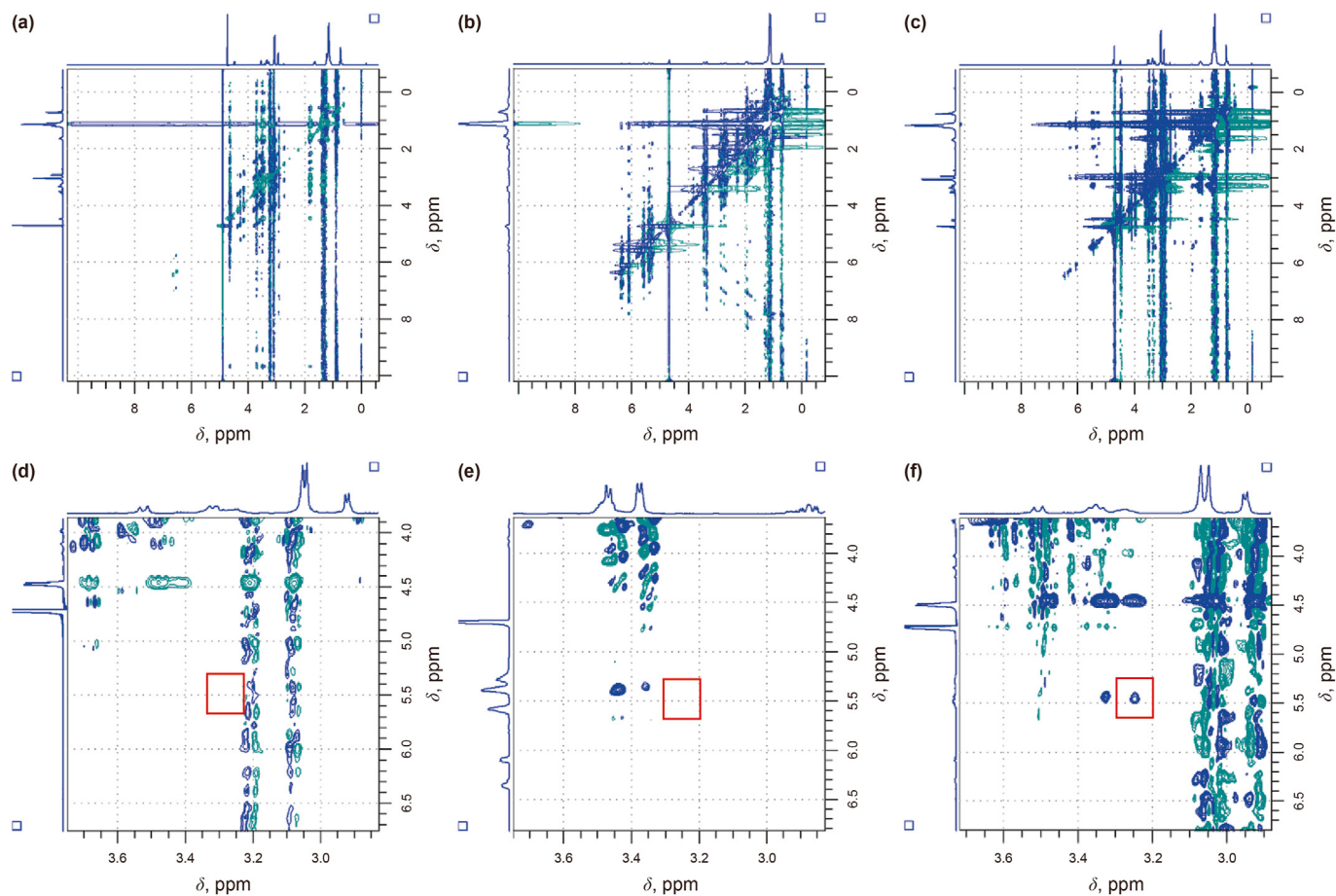


**Fig. 15.** 2D  $^1\text{H}$ - $^1\text{H}$  NOESY spectra of different surfactants: (a) HSB12; (b) AOS; (c) SA61; (d) enlarged view of HSB12; (e) enlarged view of AOS; (f) enlarged view of SA61.

### 3.6. Mobility control by compound hydroxysulfobetaine

The bulk foam test plays a pivotal role in the screening of foaming agents; however, the ability of a foaming agent to generate foam within the pores offers more informative insights (Nowrouzi et al., 2024). Therefore, the final stage of the foaming agent screening process involves conducting flow experiments (Hanamertani et al., 2021; Hemmati-Sarapardeh et al., 2020). A higher apparent foam viscosity observed in the pore medium indicates increased resistance, reduced relative mobility, and enhanced performance of the foaming agent (Nazari et al., 2022). These flow experiments effectively reflect both the adsorption and foaming abilities of the foaming agent within the core. It is worth noting that flow experiments may not necessarily correspond to static bulk foam; hence it is imperative to conduct flow experiments alongside traditional bulk foam testing.

Under controlled conditions of a fixed gas–liquid ratio of 4:1, an oven temperature set at 130 °C, and a back pressure maintained at 10 MPa, the solution of foaming agent and gas were systematically injected into Berea cores possessing varying permeabilities. The foaming ability and foam plugging performance of HSB12 and SA61, with different concentrations tested in cores exhibiting diverse permeabilities, were comprehensively evaluated as depicted in Fig. 16.

The presence of foam in the core resulted in an increased resistance to gas flow, as evidenced by a higher resistance factor, an elevated apparent viscosity, and a reduced relative mobility. This can be attributed to the combined effects of the flow resistance offered by the liquid lamellae within the foam while passing through a capillary, as well as the surface tension gradient when a liquid slug is swept from the front of a bubble and accumulates behind it (Hirasaki and Lawson, 1985). As shown in Fig. 16, under the same surfactant concentration, SA61 foam formation exhibited much higher mobility regulation compared to HSB12 foam formation. This corresponded to the excellent foam stability demonstrated by SA61 in the bulk foam test. It is widely accepted that foaming agents with foam resistance factors ranging from 10 to 100 are suitable for controlling deep profiles. Heller et al. (1985) suggested that foams effectively regulating gas mobility can reduce the gas relative mobility (the ratio of mobility to permeability) from 20 to 0.1–0.5  $\text{cP}^{-1}$ . In cores with permeabilities of 632.00 and 2005.30 mD respectively, when the concentration of SA61 exceeded 0.1 wt%, resulting foam exhibited higher viscosity and resistance factor. However, under the same conditions, the foam formed by HSB12 had an apparent viscosity lower than 1 mPa·s and a resistance factor lower than 5, indicating inadequate mobility regulation ability to meet usage requirements. These findings demonstrate that incorporating a small amount of AOS and HSB12 significantly enhanced surfactant foaming performance.

The bubble formation at the outlet of the 2005.30 mD core after injecting different concentrations of SA61 with gas at a ratio of 1:4 is shown in Fig. 17. It can be observed that the foaming properties of SA61 exhibited significant variations within the same core, ranging from intermittent and discontinuous foam produced by low-concentration foaming agents to continuous and uninterrupted foam produced by high-concentration foaming agents. As the concentration of the foaming agent increased, there was an increase in the abundance of foam generated at the exit end of the core. For a solution containing SA61 with a concentration of 0.1 wt %, although it exhibited excellent foam stability in bulk foam tests, its ability to control mobility within the core was significantly lower compared to high-concentration surfactant systems. This can be attributed to two factors: firstly, as pore-spanning lamellae propagate along pores, they undergo continuous processes such as squeezing-stretching and draining-filling due to changes in pore

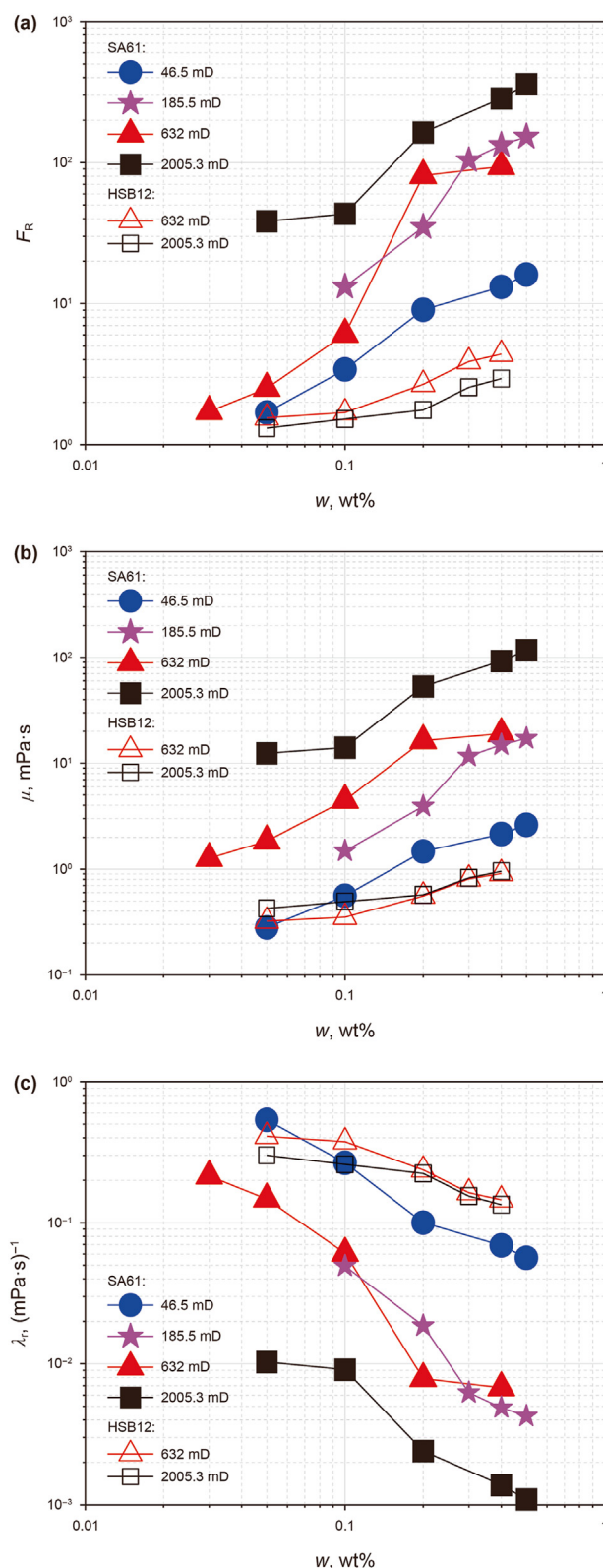


Fig. 16. Evaluation of the mobility control ability of different concentrations ( $w$ ) of SA61 and HSB12 in cores with varying permeability: (a) resistance factor ( $F_R$ ) of foam; (b) apparent viscosity ( $\mu$ ) of foam; (c) relative mobility ( $\lambda_r$ ) of foam.

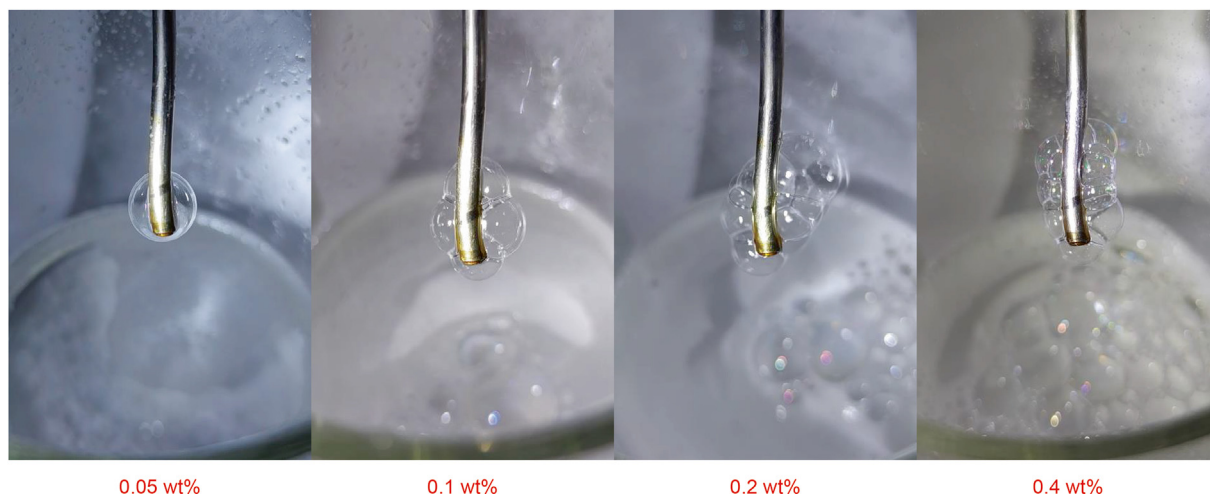


Fig. 17. Photographs of foam generation at the exit end of the 2005.30 mD core for different concentrations of SA61.

radius; higher surfactant concentrations facilitate healing surfactant solutions flowing into and stabilizing liquid films, resulting in better relative stability; secondly, higher surfactant concentrations promote easier regeneration of liquid films. These results highlighted the importance of conducting core experiments for screening optimal surfactants.

The resistance factor and apparent viscosity of the foam produced by injecting 0.05 wt% to 0.3 wt% SA61 were not significantly elevated, considering a core with permeability of 46.50 mD. This observation can be attributed to the limiting capillary pressure of the foam, which represents the maximum capillary pressure in a reservoir rock at which a flowing foam reaches its peak strength before rapid bubble coalescence occurs (Khatib et al., 1988). Khatib et al. (1988) argue that instability and coalescence are likely to occur when the entrance pressure of the foam exceeds the liquid film limit capillary pressure within pores. Unstable foams form in pores of small radii where high foam pressures exist due to higher entrance pressures compared to liquid film limit capillary pressures. Conversely, stable foams can be maintained in pores of larger radii where liquid film limit capillary pressures exceed entrance pressures. Consequently, these factors collectively contribute to relatively low surface apparent viscosity and resistance factor for foams generated under high surfactant dosages, thereby serving as an important mechanism for selective mobility control.

The superior mobility regulation ability of SA61 in the 2005.30 mD core compared to that in the 632.00 mD core is evident from Fig. 16(c), highlighting the selective effect of SA61 on mobility control (Lee et al., 1991; Li et al., 2007, 2024d). This observation indicated that within a certain permeability range, higher permeabilities resulted in more uniform foam generation and a more pronounced superimposed Jamin effect.

#### 4. Conclusions

SA61 was formed by mixing HSB12 and AOS with a mass ratio of 6:1 and exhibits good solubility in simulated formation water with a salinity of  $22 \times 10^4$  mg/L. At 130 °C and 30 MPa, the foam decay half-life of SA61 was improved by 10–25 times compared to HSB12's half-life, indicating an evident synergistic effect between dodecyl hydroxysulfobetaine and  $\alpha$ -olefin sulfonate. The surface dilatation modulus of SA61 was higher than that of HSB12 when the surfactant concentration exceeds 0.01 wt%, indicating enhanced film strength resulting from interactions between compound surfactants. This factor significantly contributed to the superior foam

stability achieved by SA61 compared to HSB12. Additionally, NMR studies of the surfactants indicated a strong interaction between HSB12 and AOS molecules in the compound surfactant system SA61. The results from core flow experiments demonstrated that the presence of foam in the core led to an increase in resistance to gas flow, as evidenced by a higher resistance factor and reduced relative mobility. Under the same concentration of surfactant, SA61 foam formation exhibited much better mobility regulation compared to HSB12 foam formation. This corresponds to the excellent foam stability demonstrated by SA61 in bulk foam tests. The concentration of injected foamer SA61 ranges 0.05–0.3 wt% for a core with permeability of 46.50 mD, resulting in lower resistance factor and apparent viscosity of the foam. The mobility regulation ability of SA61 is superior in the 2005.30 mD core compared to that in the 632.00 mD core, demonstrating the selective effect of SA61 on mobility regulation.

#### CRediT authorship contribution statement

**Long-Jie Li:** Writing – review & editing, Writing – original draft, Software, Methodology, Investigation, Data curation. **Ji-Jiang Ge:** Writing – review & editing, Writing – original draft, Validation, Supervision, Project administration, Funding acquisition, Conceptualization. **Peng-Fei Chen:** Investigation. **Peng-Ju Chu:** Investigation, Conceptualization.

#### Declaration of conflict of interest

No conflict of interest exists in the submission of this manuscript, and all authors have approved the manuscript and agree with its submission to “Petroleum Science”. We confirm that neither the manuscript nor any parts of its content are currently under consideration or published in another journal.

#### Acknowledgments

We thank Y. Yang (Chinese Academy of Sciences Qingdao Institute of Bioenergy and Bioprocess Technology Core Lab) for assistance with NMR studies. We also gratefully acknowledge the financial support from the Major Scientific and Technological Projects of CNPC (Award No. ZD2019-183-007).

## References

- Affi, H.R., Mohammadi, S., Derazi, A.M., et al., 2021. A comprehensive review on critical affecting parameters on foam stability and recent advancements for foam-based EOR scenario. *J. Mol. Liq.* 116808. <https://doi.org/10.1016/j.molliq.2021.116808>.
- Danov, K.D., Kralchevska, S.D., Kralchevsky, P.A., et al., 2004. Mixed solutions of anionic and zwitterionic surfactant (betaine): surface-tension isotherms, adsorption, and relaxation kinetics. *Langmuir* 20 (13), 5445–5453. <https://doi.org/10.1021/la0049576i>.
- Fruhner, H., Wantke, K.D., Lunkenheimer, K., 2000. Relationship between surface dilatational properties and foam stability. *Colloid. Surface.* 162 (1–3), 193–202. [https://doi.org/10.1016/S0927-7757\(99\)00202-2](https://doi.org/10.1016/S0927-7757(99)00202-2).
- Gao, F., Liu, G., Yuan, S., 2017. The effect of betaine on the foam stability: molecular simulation. *App. Surf. Sci.* 407, 156–161. <https://doi.org/10.1016/j.apsusc.2017.02.087>.
- Georgieva, D., Cagna, A., Langevin, D., 2009. Link between surface elasticity and foam stability. *Soft Matter* 5 (10), 2063–2071. <https://doi.org/10.1039/B822568K>.
- Hemmati-Sarapardeh, A., Amar, M.N., Soltanian, M.R., et al., 2020. Modeling CO<sub>2</sub> solubility in water at high pressure and temperature conditions. *Energy & Fuels* 34 (4), 4761–4776. <https://doi.org/10.1021/acs.energyfuels.0c00114>.
- Hadian Nasr, N., Mahmood, S.M., Akbari, S., et al., 2020. A comparison of foam stability at varying salinities and surfactant concentrations using bulk foam tests and sandpack flooding. *J. Petrol. Explor. Prod. Technol.* 10, 271–282. <https://doi.org/10.1007/s13202-019-0707-9>.
- Hanamertani, A.S., Saraji, S., Piri, M., 2021. The effects of in-situ emulsion formation and superficial velocity on foam performance in high-permeability porous media. *Fuel* 306, 121575. <https://doi.org/10.1016/j.fuel.2021.121575>.
- Hanamertani, A.S., Saraji, S., Piri, M., 2023. A comparative investigation of the effect of gas type on foam strength and flow behavior in tight carbonates. *Chem. Eng. Sci.* 276, 118798. <https://doi.org/10.1016/j.ces.2023.118798>.
- Heller, J.P., Lien, C.L., Kuntamukula, M.S., 1985. Foamlike dispersions for mobility control in CO<sub>2</sub> floods. *SPE J.* 25 (4), 603–613. <https://doi.org/10.2118/11233-PA>.
- Hines, J.D., Thomas, R.K., Garrett, P.R., et al., 1997. Investigation of mixing in binary surfactant solutions by surface tension and neutron reflection: anionic/nonionic and zwitterionic/nonionic mixtures. *J. Phys. Chem. B* 101 (45), 9215–9223. <https://doi.org/10.1021/jp972099a>.
- Hirasaki, G.J., Lawson, J.B., 1985. Mechanisms of foam flow in porous media: apparent viscosity in smooth capillaries. *SPE J.* 25 (2), 176–190. <https://doi.org/10.2118/12129-PA>.
- Ji, X., Tian, M., Ma, D., et al., 2018. Effects of calcium ions on the solubility and rheological behavior of a C22-tailed hydroxyl sulfobetaine surfactant in aqueous solution. *Langmuir* 34 (1), 291–301. <https://doi.org/10.1021/acs.langmuir.7b03614>.
- Jian, G., Puerto, M., Wehowsky, A., et al., 2018. Characterizing adsorption of associating surfactants on carbonates surfaces. *J. Colloid Interf. Sci.* 513, 684–692. <https://doi.org/10.1016/j.jcis.2017.11.041>.
- Khatib, Z.I., Hirasaki, G.J., Falls, A.H., 1988. Effects of capillary pressure on coalescence and phase mobilities in foams flowing through porous media. *SPE. Res. Eng.* 3 (3), 919–926. <https://doi.org/10.2118/15442-PA>.
- Koelsch, P., Motschmann, H., 2005. Relating foam lamella stability and surface dilatational rheology. *Langmuir* 21 (14), 6265–6269. <https://doi.org/10.1021/la050459c>.
- Lei, J., Gao, Y., Zhao, X., et al., 2019. The dilatational rheology and splashing behavior of ionic liquid-type imidazolium Gemini surfactant solutions: impact of alkyl chain length. *J. Mol. Liq.* 283, 725–735. <https://doi.org/10.1016/j.molliq.2019.03.146>.
- Lee, H.O., Heller, J.P., Hofer, A.M.W., 1991. Change in apparent viscosity of CO<sub>2</sub> foam with rock permeability. *SPE Res. Eng.* 6 (4), 421–428. <https://doi.org/10.2118/20194-PA>.
- Li, L., Ge, J., Chen, P., et al., 2024a. Hydroxysulfobetaine foamer for potential mobility control application in high-temperature and ultra-high salt reservoirs. *GEOEN* 241, 213167. <https://doi.org/10.1016/j.geoen.2024.213167>.
- Li, L., Ge, J., Li, K., et al., 2024b. The evaluation of dodecyl hydroxy sulfobetaine as a high-temperature and high-salinity resistant foaming agent in sandstone reservoirs. *J. Disper. Sci. Technol.* 45 (4), 759–767. <https://doi.org/10.1080/01932691.2023.2178454>.
- Li, L., Ge, J., Shi, X., et al., 2024c. Evaluation of foaming agents for high-temperature, high-pressure, and high-salinity reservoirs based on a new foam evaluator. *J. Surfactants Deterg.* 27 (3), 409–419. <https://doi.org/10.1002/jsde.12734>.
- Li, L., Ge, J., Zhang, Z., et al., 2024d. Research on compound amidohydroxysulfobetaine foamer for high-temperature and high-salinity clastic reservoirs. *Colloid. Surface. A* 135120. <https://doi.org/10.1016/j.colsurfa.2024.135120>.
- Li, Z.M., Sun, M.S., Lin, R.Y., et al., 2007. Laboratory study on foam plugging and selective divided-flow. *Acta Pet. Sin.* 28 (4), 115–118.
- Lu, J., 2024. Flow behavior and mechanism insights into nanoparticle-surfactant-stabilized nitrogen foam for enhanced oil recovery in the mature water-flooding reservoir. *ACS Omega* 9 (34), 36825–36834. <https://doi.org/10.1021/acsomega.4c06023>.
- Mannhardt, K., Novosad, J.J., 1991. Chromatographic effects in flow of a surfactant mixture in a porous sandstone. *J. Petrol. Sci. Eng.* 5 (2), 89–103. [https://doi.org/10.1016/0920-4105\(91\)90060-Z](https://doi.org/10.1016/0920-4105(91)90060-Z).
- Mclachlan, A.A., Marangoni, D.G., 2010. 1D and 2D NMR investigations of the interaction between oppositely charged polymers and surfactants. *Can. J. Chem.* 88, 124–134. <https://doi.org/10.1139/V09-039>.
- Metin, C.O., Baran, J.R., Nguyen, Q.P., 2012. Adsorption of surface functionalized silica nanoparticles onto mineral surfaces and decane/water interface. *J. Nanopart. Res.* 14, 1246. <https://doi.org/10.1007/s11051-012-1246-1>.
- Milton, J.R., Joy, T.K., translated by Cui, Z.G., Jiang, J.Z., 2015. *Surfactants and Interfacial Phenomena*. Chemical Industry Press, pp. 292–293.
- Mumtaz, M., Tan, I.M., Mushtaq, M., 2015. Synergistic effects of surfactants mixture for foam stability measurements for enhanced oil recovery applications. In: *SPE Saudi Arabia Section Annual Technical Symposium and Exhibition*. <https://doi.org/10.2118/178475-MS>.
- Nazari, N., Almajid, M.M., Kovscek, A.R., 2022. Mechanistic modeling and measurement of foamed gas flow resistance in fractures. *Adv. Water Resour.* 162, 104154. <https://doi.org/10.1016/j.advwatres.2022.104154>.
- Nowrouzi, I., Mohammadi, A.H., Khaksar Manshad, A., 2024. A non-ionic green surfactant extracted from the Anabasis setifera plant for improving bulk properties of CO<sub>2</sub>-foam in the process of enhanced oil recovery from carbonate reservoirs. *Can. J. Chem. Eng.* <https://doi.org/10.1002/cjce.25401>.
- Parra, J.G., Domínguez, H., Aray, Y., et al., 2019. Structural and interfacial properties of the CO<sub>2</sub>-in-water foams prepared with sodium dodecyl sulfate (SDS): a molecular dynamics simulation study. *Colloid. Surface. A* 578, 123615. <https://doi.org/10.1016/j.colsurfa.2019.123615>.
- Pan, X., Yang, F., Chen, S., et al., 2018. Cooperative effects of zwitterionic-ionic surfactant mixtures on the interfacial water structure revealed by sum frequency generation vibrational spectroscopy. *Langmuir* 34 (18), 5273–5278. <https://doi.org/10.1021/acs.langmuir.8b00178>.
- Qi, C., Zhang, R., Jia, K., et al., 2016. Molecular dynamics simulations and 2D-NOESY spectroscopy studied on conformational features of ACE-inhibitory tripeptide Gly-Glu-Phe in aqueous and DMSO solutions. *J. Mol. Liq.* 224, 1233–1241. <https://doi.org/10.1016/j.molliq.2016.10.107>.
- Q/SH1020 2191–2013, 2013. *Technical requirements for the selection of surfactants for oil drive*. Shengli Petroleum Administration of Sinopec Group.
- Shu, N.K., Xu, Z.C., Gong, Q.T., et al., 2021. Effect of electrolyte on the surface dilatational rheological properties of branched cationic surfactant. *Colloid. Surface. A* 627, 127170. <https://doi.org/10.1016/j.colsurfa.2021.127170>.
- Simjoo, M., Rezaei, T., Andrianov, A., et al., 2013. Foam stability in the presence of oil: effect of surfactant concentration and oil type. *Colloid. Surface. A* 438, 148–158. <https://doi.org/10.1016/j.colsurfa.2013.05.062>.
- Stournas, S., 1984. A novel class of surfactants with extreme brine resistance and its potential application in enhanced oil recovery. In: *SPE Annual Technical Conference and Exhibition*. <https://doi.org/10.2118/13029-MS>.
- Syed, A.H., Idris, A.K., Mohshim, D.F., et al., 2019. Influence of lauryl betaine on aqueous solution stability, foamability and foam stability. *J. Petrol. Explor. Prod. Technol.* 9 (4), 2659–2665. <https://doi.org/10.1007/s13202-019-0652-7>.
- Tsujii, K., Okahashi, K., Takeuchi, T., 1982. Addition-compound formation between anionic and zwitter-ionic surfactants in water. *J. Phys. Chem.* 86 (8), 1437–1441. <https://doi.org/10.1021/j100397a045>.
- Wang, H., Liu, J., Yang, Q., et al., 2021. Study on the influence of the external conditions and internal components on foam performance in gas recovery. *Chem. Eng. Sci.* 231, 116279. <https://doi.org/10.1016/j.ces.2020.116279>.
- Wang, L., Asthagiri, D., Zeng, Y., et al., 2017. Simulation studies on the role of lauryl betaine in modulating the stability of AOS surfactant-stabilized foams used in enhanced oil recovery. *Energy Fuels* 31 (2), 1512–1518. <https://doi.org/10.1021/acs.energyfuels.6b03186>.
- Weaire, D., Hutzler, S., Verbist, G., et al., 1997. A review of foam drainage. *Adv. Chem. Phys.* 102, 315–374. <https://doi.org/10.1002/9780470141618>.
- Xiong, D., Ahmed, S., Alameri, W., et al., 2022. Experimental investigation of foam flooding performance in bulk and porous media for carbonates under harsh conditions. In: *SPE Western Regional Meeting*. <https://doi.org/10.2118/209326-MS>.
- Xu, X.G., Zhang, P., Zhang, X.W., et al., 2024. Foam channeling blocking technology mechanism and new progress in fractured low permeability/tight reservoirs. *Oilfield Chem.* 41 (1), 167–178. <https://doi.org/10.19346/j.cnki.1000-4092.2024.01.023>.
- Yu, Y., Soukup, Z.A., Saraji, S., 2019. An experimental study of in-situ foam rheology: effect of stabilizing and destabilizing agents. *Colloid. Surface. A* 578, 123548. <https://doi.org/10.1016/j.colsurfa.2019.06.014>.
- Yan, F., Zhang, L., Zhao, R.H., et al., 2012. Surface dilatational rheological and foam properties of aromatic side chained N-acyltaurate amphiphiles. *Colloid. Surface. A* 396, 317–327. <https://doi.org/10.1016/j.colsurfa.2012.01.016Gettrightsandcontent>.
- Yin, D.X., Ma, P.S., Xia, S.Q., 2007. Progress on methods for measuring surface tension of liquids. *Bull. Sci. Technol.* 23 (3), 424–433.
- Zhao, Z., Wang, Q.F., 2010. Progress on methods of measuring surface active agent's critical micelle concentration. *Practical Pharmacy and Clinical Remedies* 13 (2), 140–144.
- Zhou, J.M., Srivastava, M., Hahn, R., et al., 2020. Evaluation of an amphoteric surfactant for CO<sub>2</sub> foam applications: a comparative study. In: *SPE Improved Oil Recovery Conference*. <https://doi.org/10.2118/200315-MS>.
- Zhu, H.J., Yang, P.H., 1994. Effect of dynamic interfacial tension phenomenon on oil drive efficiency in chemical drive. *Petrol. Explor. Dev.* 21 (2), 74–80. [https://kns.cnki.net/kcms2/article/abstract?v=3uoqIhG8C44YLTOATRkKjkgKvIT9NkGsvn6cq9Bo2Rg3UOyq6jPzXlnwKU3sEU8jGdUWKorDV15IogWDEYtjQHWVFW\\_gv&uniplatform](https://kns.cnki.net/kcms2/article/abstract?v=3uoqIhG8C44YLTOATRkKjkgKvIT9NkGsvn6cq9Bo2Rg3UOyq6jPzXlnwKU3sEU8jGdUWKorDV15IogWDEYtjQHWVFW_gv&uniplatform).
- Zhang, T., Ge, J., Li, L., et al., 2023. Synergism between betaine surfactants under high-salt conditions. *J. Disper. Sci. Technol.* 45 (1), 39–47. <https://doi.org/10.1080/01932691.2022.2125877>.